Research Square

Preprints are preliminary reports that have not undergone peer review.
They should not be considered conclusive, used to inform clinical practice,
or referenced by the media as validated information.

Projected response of extreme precipitation to global warming levels in Northwest Africa

Abdelaziz CHAQDID

abdelazizchaqdid@gmail.com

King Abdullah University of Science and Technology https://orcid.org/0000-0001-9695-9846

Yeon-Woo Choi

Institute of Human Complexity and Systems Science, Yonsei University, Incheon, Republic of Korea.
https://orcid.org/0000-0002-3400-6705

Abdelouahad El Fatimy

School of Applied and Engineering Physics, Mohammed VI Polytechnic University
https://orcid.org/0000-0001-6500-7762

Elfatih A. B. Eltahir

Ralph M. Parsons Laboratory, Massachusetts Institute of Technology, Cambridge, MA, 02139, USA.
https://orcid.org/0000-0002-6148-7997

Nabil El Moçayd

International Water Research Institute, Mohammed VI Polytechnic University, Ben Guerir, Morocco
https://orcid.org/0000-0002-3258-8537

Research Article

Keywords: extreme precipitation, Northwest Africa, Atlas Mountains, MRCM, CMIP6, bias correction

Posted Date: October 28th, 2026

DOI: https://doi.org/10.21203/rs.3.rs-11349496/v2

License: This work is licensed under a Creative Commons Attribution 4.0 International License.
Read Full License

Additional Declarations: The authors declare no competing interests.

Projected response of extreme precipitation to global warming levels in Northwest Africa

Abdelaziz Chaqdid[1], Yeon-Woo Choi[2,4], Abdelouahad El Fatimy[1], Elfatih A. B. Eltahir[2], and Nabil El Moçayd[3]

[1]School of Applied and Engineering Physics, Mohammed VI Polytechnic University, Ben Guerir, Morocco.

[2]Ralph M. Parsons Laboratory, Massachusetts Institute of Technology, Cambridge, MA, 02139, USA.

[3]International Water Research Institute, Mohammed VI Polytechnic University, Ben Guerir, Morocco.

[4]Institute of Human Complexity and Systems Science, Yonsei University, Incheon, Republic of Korea.

Abstract

This study investigates projected changes in extreme precipitation over Northwest Africa at global warming levels (GWLs) of 1.5–4°C using a multi-model ensemble of regional climate simulations conducted with the MIT Regional Climate Model (MRCM) at 10-km horizontal resolution. Our results reveal a nonlinear response of extreme precipitation to increasing warming levels. Across most of Northwest Africa, both the frequency and intensity of extreme precipitation are projected to decline under all warming scenarios, with reductions becoming particularly pronounced at higher GWLs (3–4°C). While the broader region follows a drying trend, a notable exception occurs over the Moroccan Atlas Mountains. In this region, moderate warming (GWL1.5–2°C) produces a robust intensification of extreme precipitation across all simulations, followed by a transition to drying at higher warming levels. This orographic anomaly may reflect a two-stage response. Lower warming levels enhance moisture-driven intensification through orographic lifting, whereas higher warming levels lead to large-scale dynamical suppression. These findings identify the Atlas Mountains as an early-warming hotspot and indicate that, beyond 2 °C of warming, extreme precipitation declines region-wide, with important implications for water resource planning.

Keywords: extreme precipitation; Northwest Africa; Atlas Mountains; MRCM; CMIP6; bias correction

1 Introduction

Northwest Africa, including Morocco, sits within the Mediterranean climate-change hotspot (Cos et al., 2022). Observations and climate models indicate a marked decline in mean precipitation, especially in winter—the key recharge season for rivers, reservoirs, and aquifers. Recent high-resolution regional simulations projects sharp reductions in winter (−22%) and spring (−34%) precipitation over Morocco's major basins, driven by circulation changes that favor Saharan dry-air intrusions and a poleward shift of storm activity (Tuel and Eltahir, 2020; Tuel et al., 2021). Prolonged drought thereby accentuates the long-recognized sensitivity of the region to North Atlantic variability and to orographic controls, compounding vulnerability to water stress (Driouech et al., 2010; Hssaisoune et al., 2020).

Amid this long-term drying, extreme precipitation (EP) exerts contrasting pressures on society and water systems across the region, bringing both relief and risks. While EP events can temporarily fill reservoirs and aquifers in otherwise depleted basins (Taylor et al., 2013), they also trigger destructive flooding, including flash floods, that severely damage communities and infrastructure (Driouech et al., 2010; Bouaicha and Benabdelfadel, 2010). Recent floods, such as in southern Morocco in September 2024, highlight this dual vulnerability, where long-lasting droughts are abruptly interrupted by severe storms (General Directorate of Meteorology, 2024). Projections for the High Atlas also indicate declining snow cover and changing seasonal runoff patterns (Tuel et al., 2022), further limiting water availability and underscoring the need to understand how EP will develop in the future.

Worldwide, the intensity of heavy rainfall increases with warming to an extent that scales with humidity (about 6–7% /K), but the regional effects depend heavily on circulation and topography (O'Gorman, 2015). The IPCC's Sixth Assessment Report (IPCC, 2022) concludes that even small increases in global warming produce statistically significant changes in extreme events, but regional EP responses reflect a balance between thermodynamic gain and circulation shifts (Seneviratne et al., 2021). In the Mediterranean, multi-model

analyses show "contrasting trends": an intensification of EP in the northern sub-basins, but a non-significant increase or even decreasing EP in the southern sectors, where drought and fewer rainy days prevail (Tramblay and Somot, 2018). For Africa, coordinated CMIP6 and Coordinated Regional Downscaling Experiment (CORDEX) comparisons point to a higher rainfall intensity with fewer rainy days and longer dry spells in the Atlas region, a combination with profound effects on both flood risk and water supply reliability (Dosio et al., 2021).

These projections of changes in EP are subject to considerable uncertainty. According to Hawkins and Sutton (2009), this uncertainty rises primarily from three sources: model uncertainty, scenario uncertainty and internal variability. In Northwest Africa, model uncertainty is particularly important and largely stems from the coarse resolution of global climate models (GCMs), which do not adequately resolve the region's complex topography, oceanic influences, and local convective storms that are critical for heavy rainfall (Seneviratne et al., 2021; Chaqdid et al., 2026). This leads to substantial inter-model differences in projected future atmospheric circulation patterns that strongly influence Moroccan EP, such as the North Atlantic Oscillation and Mediterranean storm systems (Gadouali et al., 2020; Chaqdid et al., 2023). Although heavy precipitation is generally expected to intensify from a thermodynamic perspective, the magnitude and spatial patterns of projected changes over Morocco remain highly uncertain (Tramblay et al., 2012). Moreover, the region's sparse observation network hinders robust evaluation and bias correction of climate simulations (Tuel and Moçayd, 2023).

To reduce these uncertainties, especially those stemming from model constraints, regional climate downscaling has proven to be a critical methodological advance (Giorgi, 2019). High-resolution dynamical downscaling enhances the representation of localized convective processes and complex topography, improving simulation of heavy precipitation events and reducing model biases (Torma et al., 2015). Complementing this, recent climate research increasingly adopts the Global Warming Levels (GWLs) framework, which evaluates regional climate responses based on incremental increases in global mean temperature relative to pre-industrial

levels (e.g., 1.5 °C, 2 °C, 3 °C), rather than specific time horizons tied to emissions scenarios. This approach, now standard in the IPCC's Sixth Assessment Report (IPCC, 2022), allows for a direct comparison of the regional impacts of different models and scenarios, as the timing of each GWL may vary depending on the emission path, but the associated climate responses remain physically consistent within the same model (IPCC, 2022).

Previous downscaling studies on Morocco assessed the performance of regional climate models (RCMs) and projected changes in mean climate and ETCCDI indices, confirming warming, fewer rainy days, and longer dry spells, but reporting heterogeneous results for EP metrics, highlighting model dependency and methodological choices (Tramblay et al., 2013; Filahi et al., 2016; Khomsi et al., 2016). At the regional scale, Tuel et al. (2021) used the high-resolution MIT Regional Climate Model (MRCM) to identify robust drying mechanisms and spatial gradients over Iberia and Northwest Africa. However, they did not assess how the frequency and intensity of EP respond at fixed global warming levels (GWLs), nor did they characterize EP hotspots within northwest Africa beyond basin-mean conditions. Our study addresses these gaps by following the workflow summarized in Figure 1 and examines two key questions: *(i)* how EP indices over Northwest Africa scale with projected global warming, and *(ii)* whether these changes occur uniformly across the region or reveal emerging hotspots.

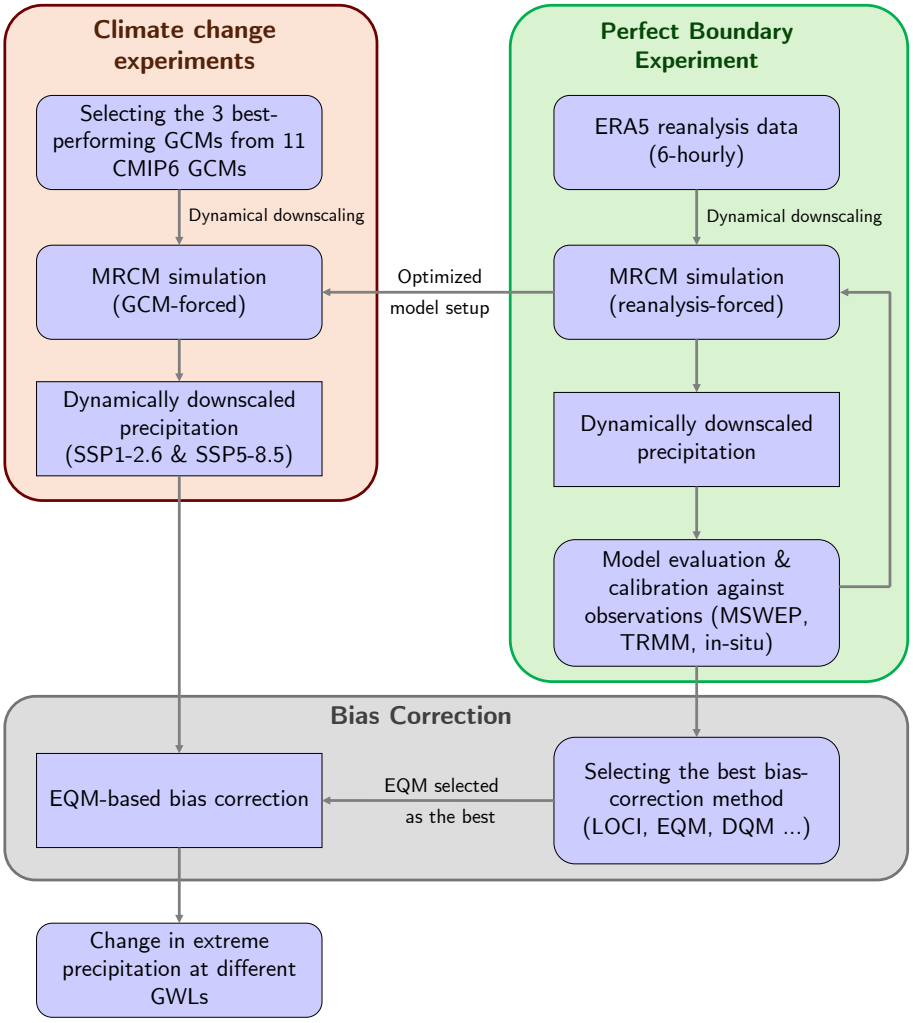


Figure 1: Flowchart of data and methodology

This paper is structured as follows: Section 2 describes the study area, the data sets used and the modeling framework. It outlines the main features of Morocco and the Atlas Mountains, explains the observational and model data, and describes the MIT Regional Climate Model (MRCM) and the selection of CMIP6 GCMs used as boundary conditions. In addition, the experimental design, the definition and bias correction of EP indices and the global warming level (GWL) framework are presented. Section 3 reports on the main findings, including the evaluation of model performance, the verification of bias-corrected MRCM simulations, and the predicted changes in frequency, intensity, and contribution of

EP events under projected global warming. Section 4 discusses the broader impact of these results on hydroclimatic risk and water availability. Finally, Section 5 summarizes the main conclusions and outlines perspectives for future research.

2 Data and Materials

2.1 Study area: Morocco and the Atlas Mountains

The study area extends across Northwestern Africa (approximately 18°W–11.5°E and 20.5°–38°N), covering Morocco, parts of Algeria, and Tunisia (see Figure 2). This domain captures the transition from the Atlantic and Mediterranean coasts, across the Atlas Mountains, into the Sahara. Model selection, downscaling, bias correction, and evaluation are applied uniformly across the full domain, with additional tuning over Morocco. We report domain-wide results and highlight Morocco as a focal subregion given the availability of in situ data and its regional importance. Within this domain, we focus on key river basins and densely populated corridors stretching from the Atlantic lowlands to the interior plateaus. The broader domain is maintained to capture moisture transport from the Atlantic and Mediterranean and its interaction with the full Atlas range, an important dynamical control on the regional climate.

The Atlas Mountains are the dominant physical feature of the domain, consisting of the Rif, Middle, High (peaking at Jebel Toubkal, 4167 m), and Anti-Atlas ranges in Morocco, continuing eastward as the Tell and Saharan Atlas. These mountains play a major role in shaping the regional climate through processes explicitly represented in our configuration: orographic uplift on windward slopes, rain-shadow and foehn effects on leeward sides, barrier jets and gap-flow channeling, coastal land–sea-breeze interactions, episodic lee cyclogenesis over the High Plateaus, and winter snow accumulation followed by spring melt in the High Atlas. Collectively, these processes generate strong spatial and seasonal gradients in temperature and precipitation that coarse global climate models cannot resolve.

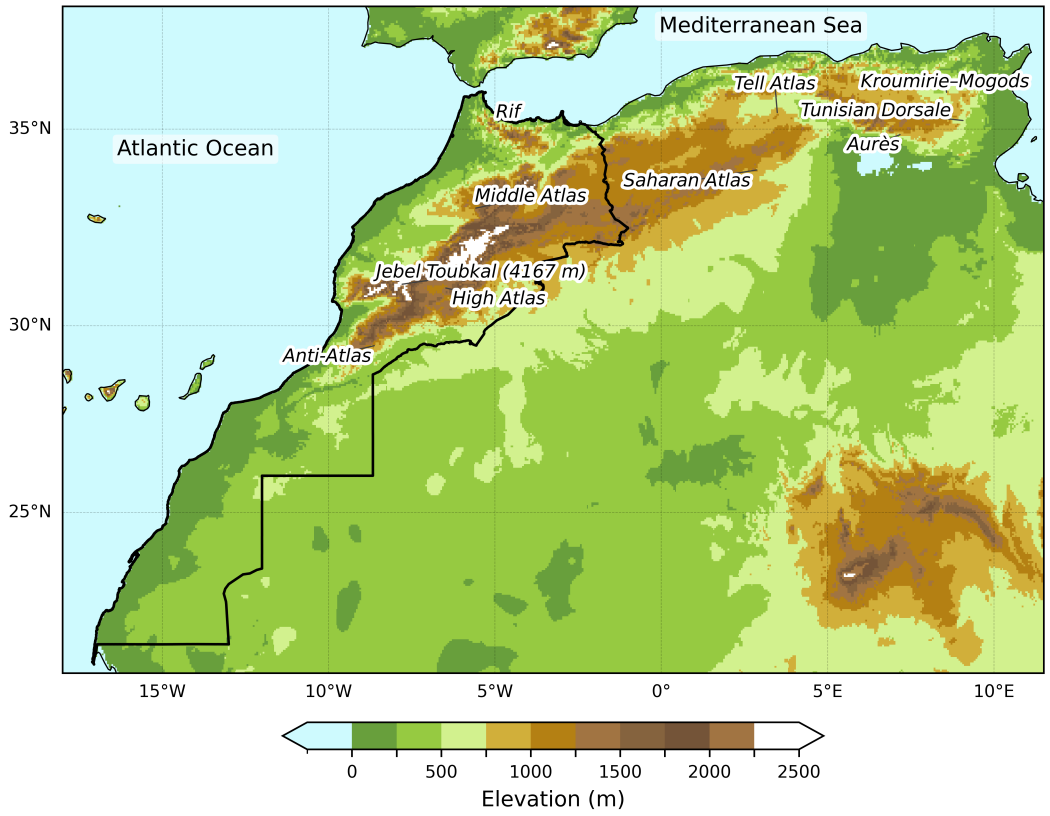


Figure 2: Topography of the study area (Northwest Africa), highlighting Morocco and the Atlas ranges that shape regional climate and elevation gradients.

2.2 Data

This study uses several datasets to address four main tasks: (i) Model selection uses daily precipitation from Multi-Source Weighted-Ensemble Precipitation (MSWEP) (0.1° resolution; Beck et al., 2019) as observational baselines, and monthly precipitation from an 11-member CMIP6 ensemble for 1979–2014. All 11 models are taken from the same experiment (historical) and ensemble member (r1i1p1f1): MIROC6, MPI-ESM1-2-HR, EC-Earth3-Veg, NESM3, NorESM2-LM, IPSL-CM6A-LR, NorESM2-MM, MRI-ESM2-0, CMCC-ESM2, BCC-CSM2-MR, and CMCC-CM2-SR5. (ii) For the reanalysis ("perfect-boundary") experiment, lateral boundary conditions (LBCs) are taken from ERA5 (Hersbach et al., 2020) at 6-hourly time steps, 0.25° horizontal resolution, and 37 vertical levels (winds `ua`, `va`; air temperature `ta`; specific humidity `hus`; surface pressure `ps`), complemented by 1° weekly sea-surface

temperature (SST) from NOAA OISST (Reynolds et al., 2002). In addition to MSWEP, we evaluate MRCM's ability to simulate the precipitation regime over Morocco and Northwest Africa using multiple datasets, including ERA5 reanalysis precipitation (0.25°); the station-based, gridded TerraClimate product (monthly, ∼4 km; Abatzoglou et al., 2018); the satellite-based TRMM precipitation product (0.25°. Huffman et al., 2007), and representative in-situ observation stations from Tuel and Moçayd (2023). (iii) For climate-change experiments, the same set of LBC variables and lower-boundary SST are extracted at 6-hourly resolution from the three selected CMIP6 GCMs (MPI-ESM1-2-HR, EC-Earth3-Veg, and IPSL-CM6A-LR; selection method described in Section 2.4). For all three GCMs, historical forcing spans 1975–2014; scenario forcing spans 2015–2100 under SSP1-2.6 and SSP5-8.5; one ensemble member (r1i1p1f1) is used per GCM. (iv) Bias correction of precipitation projections uses MSWEP as the reference. Parameters are calibrated over 1979–2014 and then applied consistently to future periods, as detailed in Section 2.7. Throughout the study, MSWEP serves as the primary reference for precipitation: it is used to calibrate the RCM over Morocco, to evaluate and select GCM forcings, and to perform bias correction. This choice is justified by the scarcity and uneven spatial distribution of weather stations in Morocco and is supported by Tuel and Moçayd (2023), who showed that—among nine gridded products evaluated against in-situ observations—MSWEP performs best for EP in Morocco.

2.3 MIT regional climate model (MRCM)

MRCM is a hydrostatic, three–dimensional regional climate model derived from the ICTP RegCM3 dynamical core (Pal et al., 2007), but upgraded with targeted physics developments designed to improve land–atmosphere coupling, convective processes, and boundary layer structure. A key element is the coupling to the Integrated Biosphere Simulator (IBIS) land surface scheme (Foley et al., 1996; Winter et al., 2009), which replaces the legacy BATS formulation used in RegCM3 and yields more realistic surface energy and water budgets over vegetated and semi–arid terrains (Im et al., 2014). Additional improvements include a revised

surface albedo prescription and an irrigation module tailored for arid regions (Marcella and Eltahir, 2012, 2014), updates to the convective cloud and rainfall autoconversion schemes (Gianotti, 2012; Gianotti and Eltahir, 2014a,b), and modified boundary layer height and low–cloud parameterizations (Gianotti, 2012).

Consistent with Tuel and Eltahir (2020) and Pal and Eltahir (2016), our baseline physics suite comprises IBIS for land surface processes (Winter et al., 2009); the SUBEX moisture scheme for large–scale condensation and microphysics (Pal et al., 2000); the NCAR CCM3 radiation package (Kiehl et al., 1998); a nonlocal planetary boundary layer scheme (Holtslag and Boville, 1993); and the bulk air–sea flux algorithm of Zeng et al. (1998). Deep convection is represented with the Grell scheme using Fritsch–Chappell closure, in line with prior MRCM applications over drylands (Pal and Eltahir, 2016). Simulations are conducted at 10 km horizontal resolution, which is sufficient to resolve first–order orographic gradients across the Atlas ranges and land–sea contrasts along the Mediterranean and Atlantic coasts of Northwest Africa, features that modulate EP.

Relative to Tuel and Eltahir (2020), we restrict modifications to a light fine–tuning of the SUBEX large–scale condensation and microphysics scheme, aimed at improving the timing and intensity of wet-season precipitation while preserving large-scale fidelity. Specifically, we adjusted a small set of SUBEX parameters that regulate the onset and efficiency of cloud water conversion to rain (e.g., autoconversion threshold and rate constants, and accretion efficiency), after brief sensitivity tests against observed daily precipitation distributions over Morocco. No structural changes to the physics were introduced.

2.4 GCM selection

For GCM selection, we rank models based on their ability to reproduce the observed seasonal cycle of precipitation over the full domain (Figure 1). For each of the 11 CMIP6 models described in Section 2.2, we extract monthly precipitation for 1979–2014, compute spatial

averages over the study area, and compute climatological monthly means (see seasonality plots in Figure S2 in the Supplementary Materials). We then calculate two evaluation metrics—the Pearson correlation and a relative RMSE—between the modeled and observed seasonal cycles. Let $\overline{M}(m)$ and $\overline{O}(m)$ denote the model and observed Morocco-mean monthly precipitation climatologies for month $m = 1, \ldots, 12$. The correlation is taken across the 12 months (between the two 12-element vectors):

$$\mu^{\text{mod}} = \frac{1}{12}\sum_{m=1}^{12}\overline{M}(m), \qquad \mu^{\text{obs}} = \frac{1}{12}\sum_{m=1}^{12}\overline{O}(m), \tag{1}$$

$$\rho = \frac{\sum_{m=1}^{12}\left(\overline{M}(m)-\mu^{\text{mod}}\right)\left(\overline{O}(m)-\mu^{\text{obs}}\right)}{\sqrt{\sum_{m=1}^{12}\left(\overline{M}(m)-\mu^{\text{mod}}\right)^2}\sqrt{\sum_{m=1}^{12}\left(\overline{O}(m)-\mu^{\text{obs}}\right)^2}}. \tag{2}$$

The relative RMSE is normalized by the observed seasonal mean:

$$\text{rRMSE} = \frac{\sqrt{\frac{1}{12}\sum_{m=1}^{12}\left[\overline{M}(m)-\overline{O}(m)\right]^2}}{\mu^{\text{obs}}}. \tag{3}$$

Models are ranked by ρ (descending) and by rRMSE (ascending); the *mean rank* is the arithmetic mean of these two ranks (ties broken by smaller rRMSE). The resulting scores (Table 1) single out three consistently strong models for simulating precipitation over Morocco—**EC-Earth3-Veg** (highest ρ and second-lowest rRMSE; mean rank **1.5**), **MPI-ESM1-2-HR** (lowest rRMSE and third-highest ρ; mean rank **2.0**), and **IPSL-CM6A-LR** (ranked 5th by ρ and 5th by rRMSE; mean rank **5.0**). Notably, Babaousmail et al. (2021) identified EC-Earth3-Veg and IPSL-CM6A-LR among the best models for reproducing rainfall patterns in North Africa. Our three selected GCMs also rank among the six top performers for Morocco in Gumus et al. (2023), who evaluated 15 CMIP6 GCMs using an ANN-based multi-model ensemble. We therefore retain these three GCMs: EC-Earth3-Veg (Döscher et al., 2022), MPI-ESM1-2-HR (Gutjahr et al., 2019), and IPSL-CM6A-LR (Boucher et al., 2020) as

boundary forcings for downscaling (historical and SSP1-2.6/SSP5-8.5 scenarios), as detailed in Section 2.5.

Model	ρ		$rRMSE$		**Mean Rank**
	Value	**Rank**	**Value**	**Rank**	
EC-Earth3-Veg	**0.481**	**1**	**0.145**	**2**	**1.5**
MPI-ESM1-2-HR	**0.473**	**3**	**0.105**	**1**	**2.0**
IPSL-CM6A-LR	**0.395**	**5**	**0.203**	**5**	**5.0**
MIROC6	0.473	2	0.223	8	5.0
BCC-CSM2-MR	0.344	9	0.193	3	6.0
CMCC-ESM2	0.421	4	0.230	9	6.5
NorESM2-LM	0.364	8	0.205	6	7.0
MRI-ESM2-0	0.364	7	0.208	7	7.0
NorESM2-MM	0.332	10	0.201	4	7.0
NESM3	0.372	6	0.253	10	8.0
CMCC-CM2-SR5	0.307	11	0.260	11	11.0

Table 1: GCM performance based on domain-mean seasonal cycle metrics (correlation and rRMSE), using MSWEP precipitation as observational baselines.

2.5 Experimental design

We adopt a two–stage strategy: (i) a reanalysis–driven "perfect–boundary" experiment to evaluate the model and set physics choices, and (ii) climate–change experiments forced by selected CMIP6 GCMs.

Stage 1: Reanalysis–driven evaluation (ERA5/MRCM): MRCM is integrated at 10 km over our study area (Figure 2) using ERA5 (Hersbach et al., 2020) as lateral boundary conditions (6-hourly fields) and weekly NOAA OISST (Reynolds et al., 2002), for 1982–2012. The year 1982 is used as spin-up and discarded. This experiment, hereafter ERA5/MRCM, is used to verify the model's ability to reproduce the regional hydroclimate and to confirm the physics choices described in Section 2.3 (with light fine–tuning restricted to SUBEX). Spatial patterns and seasonal cycle of precipitation are evaluated against multiple observational products for robustness, including weather stations, gauge–reanalysis, and gauge–satellite datasets (MSWEP, TerraClimate, TRMM).

Stage 2: GCM–driven historical and future experiments (MRCM/CMIP6): For each of the three selected GCMs (Section 2.4), one ensemble member is used to provides 6-hourly lateral boundary conditions. We perform one historical integration (1975–2014; forced by CMIP6 historical greenhouse gas concentrations) and two scenario integrations covering 2015–2100 under SSP1-2.6 and SSP5-8.5. The first simulation year of each integration is discarded as spin-up, leaving 1976–2100 (continuous integration) for analysis. Apart from boundary conditions, the model configuration is identical to ERA5/MRCM. This results in ten MRCM runs, each at 10 km resolution over the same domain; see Table 2.

Experiment	**Boundary conditions**	**Scenario**	**Simulation period**
Reanalysis downscaling	ERA5 (6-hourly) + SST	N/A	1982–2012
Climate change simulations	MPI-ESM1-2-HR	Historical	1975–2014
		SSP1-2.6	2015–2100
		SSP5-8.5	2015–2100
	EC-Earth3-Veg	Historical	1975–2014
		SSP1-2.6	2015–2100
		SSP5-8.5	2015–2100
	IPSL-CM6A-LR	Historical	1975–2014
		SSP1-2.6	2015–2100
		SSP5-8.5	2015–2100

Table 2: Summary of MRCM integrations at 10 km resolution. Boundary conditions differ by experiment, but model configuration is identical across all runs.

2.6 Extreme precipitation definition

Extremes are quantified using a compact subset of ETCCDI indices, chosen to isolate the important flood-relevant behaviors in Morocco's hydroclimate while ensuring comparability with free-running climate simulations. The set of indices includes three complementary dimensions: (i) frequency: how often heavy-precipitation days occur; (ii) intensity/accumulation: the magnitude of daily maxima and the annual totals; (iii) tail contribution: the share of seasonal/annual total values that come from the upper tail. We prefer threshold-based indices as they are interpretable, robust under moderate sample sizes, and spatially comparable;

the setting of percentile thresholds via a historical baseline separates change signals cleanly from changing climatological conditions (ETCCDI, 2009; Dunn et al., 2020). All metrics are calculated annually and seasonally from daily precipitation rates (Table 3).

Table 3: Extreme precipitation indices with brief definitions.

Index	Long name	Description
	Frequency	
R95p	Very Wet Days	Annual count of days > 95th percentile.
R99p	Extremely Wet Days	Annual count of days > 99th percentile.
	Intensity	
RX1day	Maximum 1-day precipitation	Annual maximum of daily precipitation.
SDII	Simple Daily Intensity Index	Annual mean precipitation on wet days.
PRCPTOT	Annual Total Wet-Day Precipitation	Annual total on wet days.
	Contribution	
R95pTOT	From Very Wet Days	Annual precipitation total (mm) from >95th-percentile days.
R99pTOT	From Extremely Wet Days	Annual precipitation total (mm) from >99th-percentile days.

Wet day: ≥ 1 mm; dry day: < 1 mm. Percentiles are estimated on a fixed historical reference and applied to all periods. Unless noted, indices are computed per calendar year and reported as the mean across years.

2.7 Bias correction of extreme precipitation

We evaluate a suite of bias-correction (BC) methods for their ability to correct daily precipitation biases, with emphasis on precipitation extremes (cf. inflation issues in quantile methods; Maraun, 2013). Our evaluation uses the ERA5-forced MRCM integration (1983–2022) as a controlled testbed, following the recommendation of Maraun (2016). The tested methods include: (i) simple approaches: Linear Scaling (SCALING; Lenderink et al., 2007) and Local Intensity Scaling (LOCI; Schmidli et al., 2006); (ii) advanced empirical methods: Empirical Quantile Mapping (EQM; Themeßl et al., 2012), Quantile Delta Mapping, and Detrended Quantile Mapping (DQM and QDM; Cannon et al., 2015); and (iii) advanced parametric methods: Parametric Quantile Mapping with Gamma distribution (PQM; Piani et al., 2010), PQM with GPD distribution for tails (GPQM; Gutjahr and Heinemann, 2013). Calibration

is performed over 1983–2012 (30 years) using MSWEP as reference; skill is then assessed on the unseen period 2013–2022 (10 years). The relative mean absolute bias (rMAB) is the skill metric used; evaluated for three complementary aspects of extremes: `RX1day` for intensity, `R95p` for frequency, and `R95pTOT` for contribution (see Table 3 for details).

BC method selection is conducted over Morocco only. This choice ensures computational feasibility while preserving methodological robustness. Testing seven univariate bias-correction methods on daily series at 10-km resolution over the entire model domain would be computationally demanding while offering limited additional benefit for method ranking. In contrast, Morocco encompasses the principal precipitation regimes and extremes relevant to this study, enabling a robust and representative comparison of candidate methods.

For the production runs, however, the selected bias-correction method is calibrated over the full model domain using the common reference period between MSWEP and each GCM/MRCM simulation (1979–2014). This 36-year period corresponds to the complete overlap between MSWEP and the model simulations and is therefore used in its entirety for calibration. Reiter et al. (2016) highlighted the high sensitivity of quantile mapping (QM) methods, particularly empirical quantile mapping (EQM), to the length of the calibration period and recommended using the longest available reference record. Using the full overlap period thus ensures more robust estimation of quantiles across the entire precipitation distribution. Additionally, bias correction is applied to daily precipitation separately for each calendar month to explicitly account for seasonality.

The calibrated BC method is then applied to both historical and future simulations, yielding a continuous 1995–2100 record for each GCM/MRCM simulation. The period 1995–2014 is adopted as the historical reference for computing changes in EP indices within the Global Warming Level (GWL) framework described in the next section, consistent with recent IPCC assessments and representative of present-day climatic conditions. All indices

are subsequently computed from these bias-corrected series.

2.8 Global warming levels approach

We analyze EP using the global warming level (GWL) framework: a level is reached when the 20-year running mean of global surface air temperature (GSAT), relative to 1850–1900, reaches the target warming. Conditioning on GWL shifts uncertainty from emissions pathways to the timing of when each level is reached; we therefore pool years across scenarios within each GWL. This reduces apparent scenario-dependence and allow inter-model differences to primarily reflect physical responses rather than scenario timing (IPCC, 2022). It is also policy relevant, directly mapping results to the Paris Agreement thresholds (1.5, 2 °C; UNFCCC, 2015), and physically motivated: many hydrometeorological changes, including heavy precipitation, scale approximately with warming via moisture increase (O'Gorman, 2009). We therefore report changes in EP indices at selected GWLs (1, 1.5, 2, 3, and 4 °C; see Supplementary Figure S1).

Figure S1 summarizes, for each downscaled GCM and scenario, the first 20-yr window in which a given GWL is reached; the corresponding years are listed in Table S1 (Supplementary material). For both scenarios, EC-Earth3-Veg and IPSL-CM6A-LR reach each GWL at approximately the same time, whereas MPI-ESM1-2-HR tends to lag. Under SSP5-8.5, all three exceed 2 °C by mid-century; by late century, EC-Earth3-Veg and IPSL-CM6A-LR reach 4 °C, while MPI-ESM1-2-HR does not. These windows anchor the mapping of changes in selected EP indices (Section 2.6) to specific warming levels.

3 Results

3.1 Evaluation of model performance

Prior to analyzing downscaled projections of EP, we demonstrate the ability of MRCM to reproduce the mean spatial pattern and the seasonal cycle of precipitation over Morocco

and Northwest Africa. In both the reanalysis-forced simulation (ERA5/MRCM) and the GCM-forced ensemble (ENS/MRCM), the regional model sharpens gradients and resolves orographic maxima that are muted in the raw GCM ensemble mean (ENS/GCM) (Figure 3). Resolving these coastal and orographic precipitation gradients is essential for the extremes analysis that follows. Moreover, rainfall patterns and domain-wide statistics are broadly consistent with observations (MSWEP, TerraClimate, TRMM), albeit with a wet bias along the Atlantic and Mediterranean coasts and across the Atlas ranges. The persistence of these biases in both ERA5/MRCM and ENS/MRCM likely reflects a systematic misrepresentation of subgrid scale coastal and orographic processes.

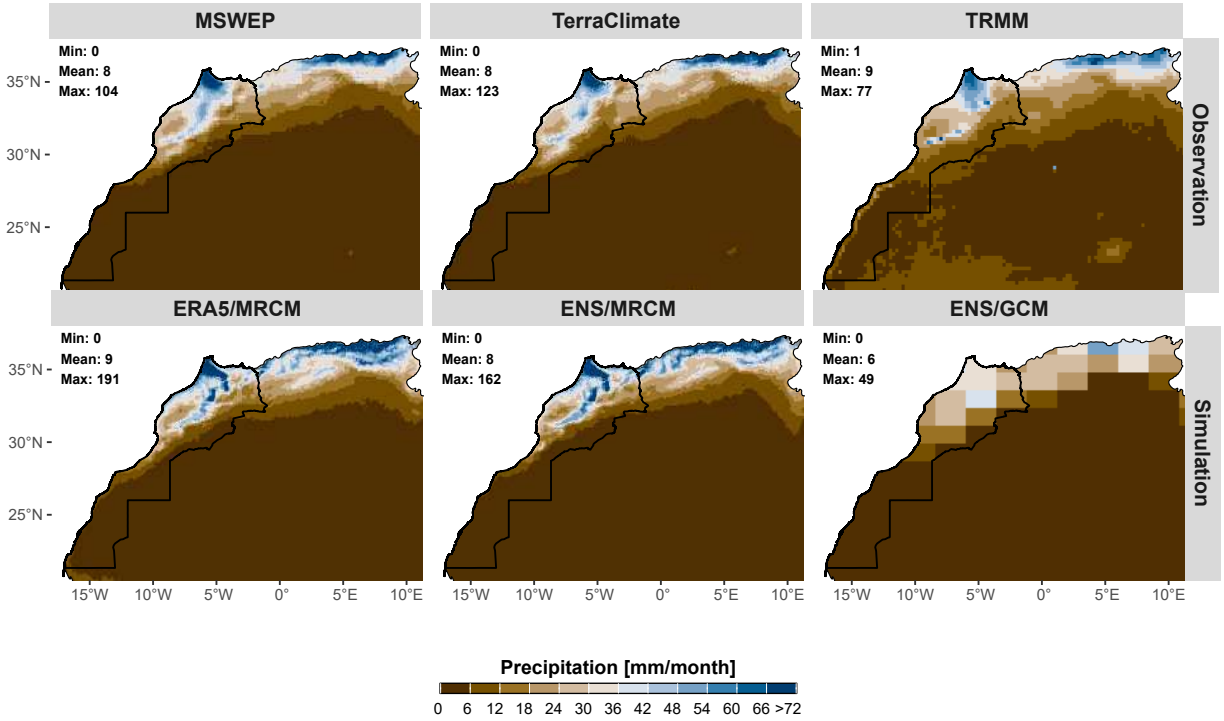


Figure 3: Climatological mean precipitation (1983–2012) across Morocco and Northwest Africa from observation-based datasets (MSWEP, TRMM, TerraClimate), ERA5-forced simulation (ERA5/MRCM), ensemble mean of the 3 GCM-forced simulations (ENS/MRCM), and ensemble mean of 11 GCMs (ENS/GCM).

Next, we assess the seasonal cycle and interannual variability of domain-mean precipitation (Figure 4). Over Morocco, ERA5/MRCM reproduces the observed winter and spring wet seasons and lies within the observational envelope for most months, with noticeable wet

bias from January to March. A similar pattern is seen over Northwest Africa, where the simulated seasonal cycle generally lies within the observed range but again exhibits a wet bias during January–May (Figure 4a). Because the bias is seasonally locked, we address it using month-specific bias correction (Section 3.2). By contrast, raw ENS/GCM substantially underestimates winter precipitation over both Morocco and the broader domain; MRCM reduces this dry bias and adds fine-scale structure, though large-scale GCM biases inevitably propagate through the lateral boundaries (see Supplementary Figure S3).

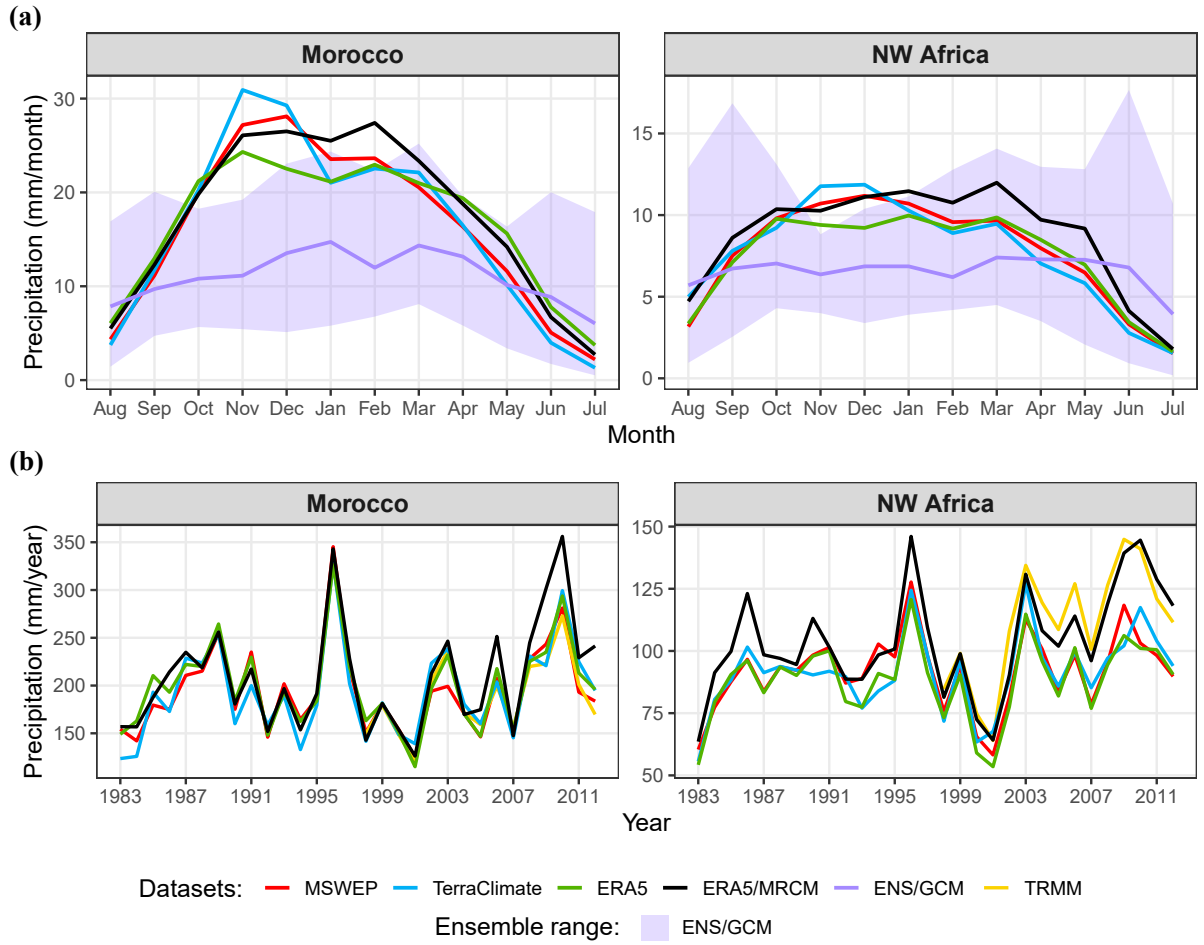


Figure 4: Monthly precipitation climatology (a) and Interannual precipitation totals (b) for the period 1983–2012 and spatially averaged over Morocco and Northwest Africa from observation-based datasets (MSWEP, TRMM, TerraClimate, raw ERA5), ERA5-forced simulation (ERA5/MRCM), and ensemble mean of 11 GCMs (ENS/GCM).

Interannual variability at the country and regional scales (Figure 4b) further supports the fidelity of MRCM. Over Morocco, year-to-year totals simulated by ERA5/MRCM fall within

the narrow observational range. Over Northwest Africa, departures are larger, reflecting sparse gauge coverage across arid interiors and the role of satellite-based products in such regions. Indeed, discrepancies are most evident during 2003–2011, when the model aligns more closely with the TRMM (satellite-based product) than with ERA5, MSWEP, or TerraClimate. Overall, the low-frequency hydroclimate signal is well captured.

Finally, we verify model behavior at the point scale using in-situ stations spanning coastal zones, the Atlas foothills, interior plains, and the southern fringe (see Supplementary Figure S4 for station locations). ERA5/MRCM reproduces the local seasonal cycle at most stations (Supplementary Figure S5); amplitude differences are largest at strongly orographic or coastal sites, consistent with the biases discussed above and with point–grid representativeness limits. At many locations (e.g., Marrakech, Agadir, Larache, Chefchaouen), MRCM improves upon the raw ERA5 seasonal cycle. The same conclusions hold for interannual variability (Supplementary Figure S6).

3.2 Verification of bias corrected MRCM runs

We evaluate seven bias-correction methods applied to ERA5/MRCM using three standard extreme-precipitation metrics: `R95p` (frequency), `R95pTOT` (contribution), and `RX1day` (intensity). Performance is assessed on a training set (1983–2012; 30 years of daily precipitation) and an independent test set (2013–2022; 10 years). Table 4 reports the relative mean absolute bias (rMAB) of each method and metric relative to MSWEP, along with a per-method mean rMAB and rank.

In training, all methods markedly reduce the raw MRCM bias: the MRCM mean rMAB of 21.2% is lowered to ∼1–6% depending on method, with nonparametric/empirical quantile approaches leading. DQM (1.1%) and EQM (1.5%) perform best, followed by PQM (3.3%), LOCI (3.8%), linear SCALING (4.4%), and GPQM (6.3%). On the unseen test set, the ordering is broadly preserved. Starting from a mean rMAB of 39.8% for MRCM, EQM

Table 4: Relative mean absolute bias (rMAB) for extreme-precipitation metrics in the training (1983-2012) and test (2013-2022) datasets. Columns are grouped by dataset; within each dataset we report the per-metric rMAB, and per-method mean rMAB and rank (lower is better).

		Train			**Test**		
Method	Metric	rMAB [%]	Mean [%]	Rank	rMAB [%]	Mean [%]	Rank
	R95N	15.7			**30.8**		
MRCM	R95P	**22.4**	**21.2**	**8**	**51.4**	**39.8**	**7**
	RX1day	**25.5**			**37.4**		
	R95N	**0.7**			**16.2**		
EQM	R95P	**0.4**	**1.5**	**2**	**23.8**	**21.3**	**1**
	RX1day	**3.3**			**24.1**		
	R95N	0.0			22.3		
DQM	R95P	0.1	1.1	1	28.9	25.3	3
	RX1day	3.3			24.8		
	R95N	1.5			16.2		
PQM	R95P	3.6	3.3	3	26.3	22.9	2
	RX1day	4.9			26.2		
	R95N	1.5			146.2		
LOCI	R95P	4.3	3.8	4	110.4	95.0	8
	RX1day	5.5			28.4		
	R95N	3.7			20.8		
SCALING	R95P	3.5	4.4	5	28.6	26.1	4
	RX1day	6.1			29.1		
	R95N	1.5			16.9		
GPQM	R95P	6.3	6.3	6	46.1	37.3	6
	RX1day	1.1			49.0		
	R95N	8.2			31.5		
DQM (alt.)	R95P	5.6	6.5	7	33.7	30.1	5
	RX1day	5.6			25.1		

achieves the lowest mean (21.3%), PQM and DQM follow (22.9–25.3%), linear scaling is modest (26.1%), GPQM is higher (37.3%), and LOCI fails out of sample (95.0%). This pattern is consistent across `R95p`, `R95pTOT`, and `RX1day` (See also Figures S7-S9 from Supplementary Materials for the spatial distribution of each method biases in the test datasets). In aggregate, EQM reduces the mean rMAB by ∼20% in training (21.2% → 1.5%) and by ∼19% in test (39.8% → 21.3%), indicating effective correction of both frequency and intensity tails without overfitting.

Having established the ranking, we examine how the leading method (EQM) alters the spatial pattern of bias. In the training set, raw MRCM exhibits a coherent wet excess along the Atlantic and Mediterranean coasts and across the Atlas for all three indices (Figure 5); EQM removes most of these biases (See also Figure S10 from Supplementary Materials for bias-corrected ENS/MRCM spatial patterns of the EP indices).

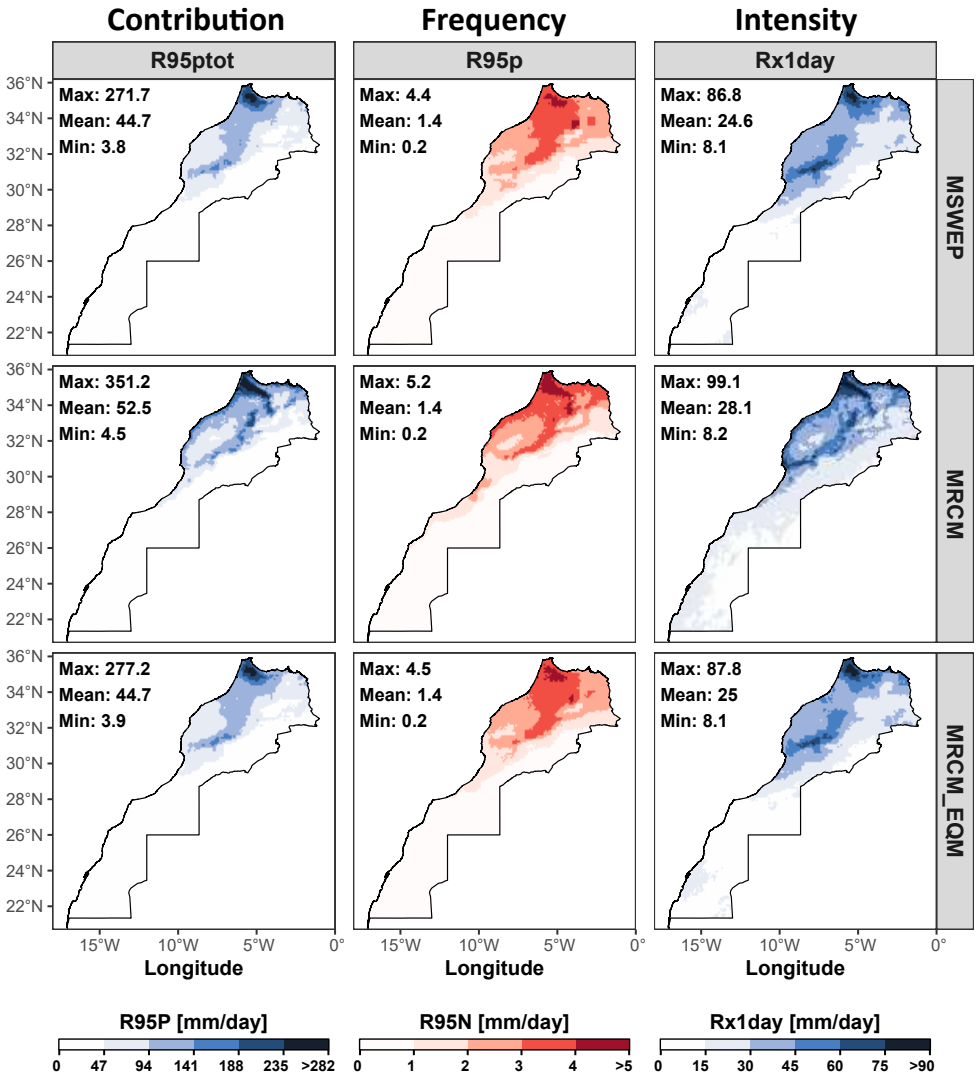


Figure 5: Climatological means of extreme-precipitation indices—`R95p`, `R95pTOT`, and `Rx1day`—computed annually from MSWEP, ERA5/MRCM, and EQM-corrected ERA5/MRCM over the training period (1983–2012).

during the independent test years (2013–2022), EQM retains most of the improvements achieved on the training period. The raw MRCM continues to show a wet bias along the

Atlantic and Mediterranean coasts for all three EP indices, but these biases are effectively removed in the bias-corrected MRCM EP fields (Figure S11). Small residual biases persist in a few areas on the test set, especially the `RX1day`; these likely reflect inconsistencies between MSWEP (used as the observational reference) and ERA5 (used to force MRCM). Overall, we remove the systematic coastal and Atlas-range wet biases while allowing the model to preserve its own dynamical response to forcings. This spatial-bias–correcting efficacy explains why EQM ranks first in the rMAB ordering in Table 4.

Our bias correction targeted not only spatial biases but also the seasonal cycle. To this end, we did not correct the full time series at once; instead, we applied the correction to daily precipitation separately for each month. This month-wise approach better reduces seasonal-cycle bias, as shown in Figure 6, which compares the observed seasonal cycle (MSWEP) with the corrected ERA5/MRCM and ENS/MRCM simulations. This bias -correction step is necessary for quantifying seasonal changes in extremes. The correction preserves phase and brings amplitudes closer to observations. Taken together with the rMAB results and the spatial diagnostics above, this supports the use of EQM-corrected fields in the extremes analysis that follows.

3.3 Future projections in extreme precipitation

Before analyzing projected changes, we first describe the present-day EP climatology of the region. Figure 7 highlights a coherent coastal-orographic band of enhanced EP activity stretching from the Atlantic façade of Morocco and the Rif, across the Middle and High Atlas, and eastward along the Tell Atlas of Algeria to northern Tunisia (Kroumirie-Mogods). Intensity metrics (`SDII`, `RX1day`) systematically peak on windward slopes exposed to Atlantic and western Mediterranean moisture fluxes, as well as in neighbouring coastal plains (e.g., Gharb-Chaouia in Morocco; Oran-Mitidja-Kabylie in Algeria; Kroumirie in Tunisia). Immediately leeward, values drop markedly across the interior plateaus (Moulouya/Oriental; Algerian High Plateaus) and south of the Saharan Atlas, consistent with strong rain-shadow effects.

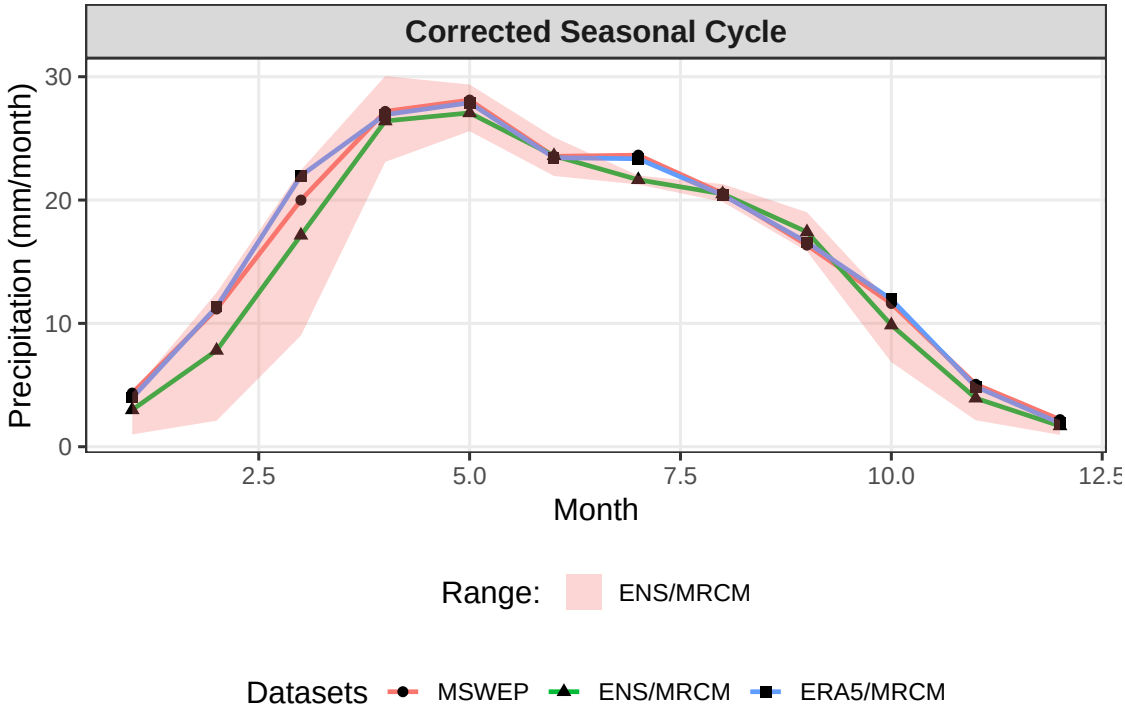


Figure 6: Morocco-mean seasonal cycle (1983–2012) from MSWEP, ERA5/MRCM, and the GCM-forced ensemble mean (ENS/MRCM); model series are shown after EQM correction.

In Morocco, `RX1day` attains maxima of about 80 mm, while `SDII` reaches roughly 12 mm/day. The lowest values are confined to pre-Saharan and southern regions. Frequency indices (`R95p`, `R99p`) display a similar west-east and coast-interior gradient. Very wet days (`R95p`) occur up to $\sim$ 5.2 days/yr, whereas extremely wet days (`R99p`) occur up to $\sim$ 1 day/yr. These events concentrate along the Atlantic-Mediterranean coastal and mountain corridor and diminish rapidly toward the semi-arid interior. Indices measuring tail contributions (`R95pTOT`, `R99pTOT`), the cumulative precipitation from days above the 95th and 99th percentiles, reinforce this pattern. Over Morocco, `R95pTOT` reaches about 274 mm (mean: 45 mm), and `R99pTOT` peaks near 83 mm (mean: 14.6 mm).

This climatological structure establishes the reference state against which changes at fixed global warming levels (GWLs) are assessed in the following sections.

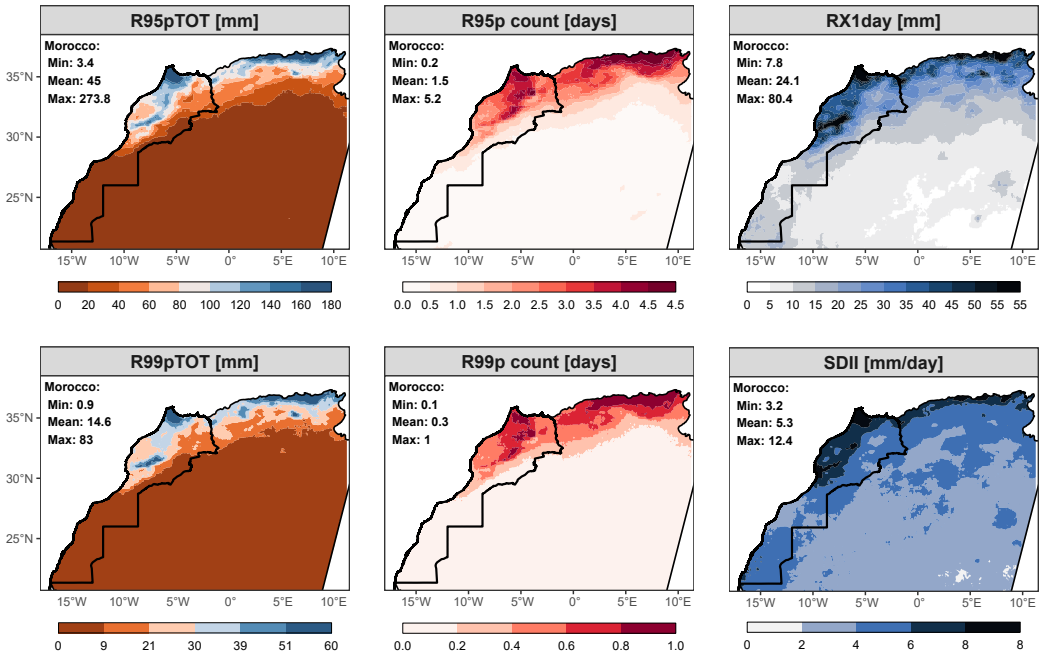


Figure 7: Spatial climatology (1979–2014) of extreme-precipitation indices from MSWEP: intensity/accumulation (`RX1day`, `SDII`); frequency (`R95p`, `R99p`); and tail contribution (`R95pTOT`, `R99pTOT`). Annotated statistics are computed over Morocco only.

3.3.1 Change in frequency

We first assess how the frequency of EP events changes across fixed GWLs. Figure 8 shows Morocco- and domain-wide projected changes in the annual counts of days exceeding the 95th and 99th wet-day percentiles at each GWL. For each level, changes are computed over the corresponding 20-year window relative to 1995–2014, with percentile thresholds defined on the reference period. A clear domain-scale pattern emerges for `R95p`: the number of very-wet days generally decreases as warming increases, with the most coherent declines confined to the coastal–mountain belt in the north (Atlantic façade, Rif–Middle/High Atlas, Tell, and Kroumirie). The black stippling (dots) marks pixels where all downscaled GCMs agree on the sign of change; stippling in Figure 8 becomes more widespread and continuous at higher GWLs, indicating strengthening robustness of the negative signal. By contrast, a localized increase appears over the southwest beginning near GWL2°C and intensifies toward GWL4°C; however, these positive patches are not stippled, implying weak inter-model

agreement and low robustness. Focusing on Morocco, the national pattern follows the domain-wide signal: at GWL1.5°C the overall decrease is weakest and largely confined to the northern Mediterranean/Atlantic littoral, while a simultaneous increase appears over parts of the High Atlas, with some stippling indicating agreement among models. As highlighted by the zoomed insets in Figure 8, the stippling over positive anomalies is more prominent for `R99p`, where the mountainous regions of Draa-Tafilalet, Beni Mellal-Khenifra, and Marrakech-Safi show denser model agreement on increasing extreme-day frequency across the Atlas interior compared to `R95p`. Notably, this High-Atlas increase fades with further warming and transitions to a decrease by GWL3°C.

For the rarer `R99p` (extremely wet days), the spatial pattern broadly echoes `R95p` but with much smaller amplitudes, reflecting sample size (rarer events). The Morocco-mean change is near zero around GWL 2 and only about −0.08 events/yr at higher GWLs (roughly −2 events per 20 years). Stippling is correspondingly sparse: where present, it most often marks negative changes along the Atlantic–Mediterranean coastal–orographic belt in the north of the domain. In contrast, a more distinct, stippled positive change than for `R95p` appears over orographically favored segments of the Atlas at GWL 1.5–2. These localized increases weaken and typically reverse by around 4 °C. Taken together, the results indicate robust decreases in the frequency of EP days along the coastal–mountain corridor as warming advances, while early Atlas enhancements in `R99p` remain localized and generally vanish by about 3 °C.

At the seasonal scale, the drying is driven by a marked reduction in October–January EP events. Both `R95p` and `R99p` show sub-baseline values in these months across all GWLs, with ensemble means (black dots) consistently below the 1995–2014 seasonal cycle (blue line) and interquartile ranges largely remaining under the baseline (Figure 9). This monthly signal matches the spatial maps: along the Atlantic–Mediterranean coastal–orographic corridor, the negative stippling marks grid cells where all members agree on a decrease; accordingly, the monthly boxes lie completely below the baseline, confirming cross-member reductions

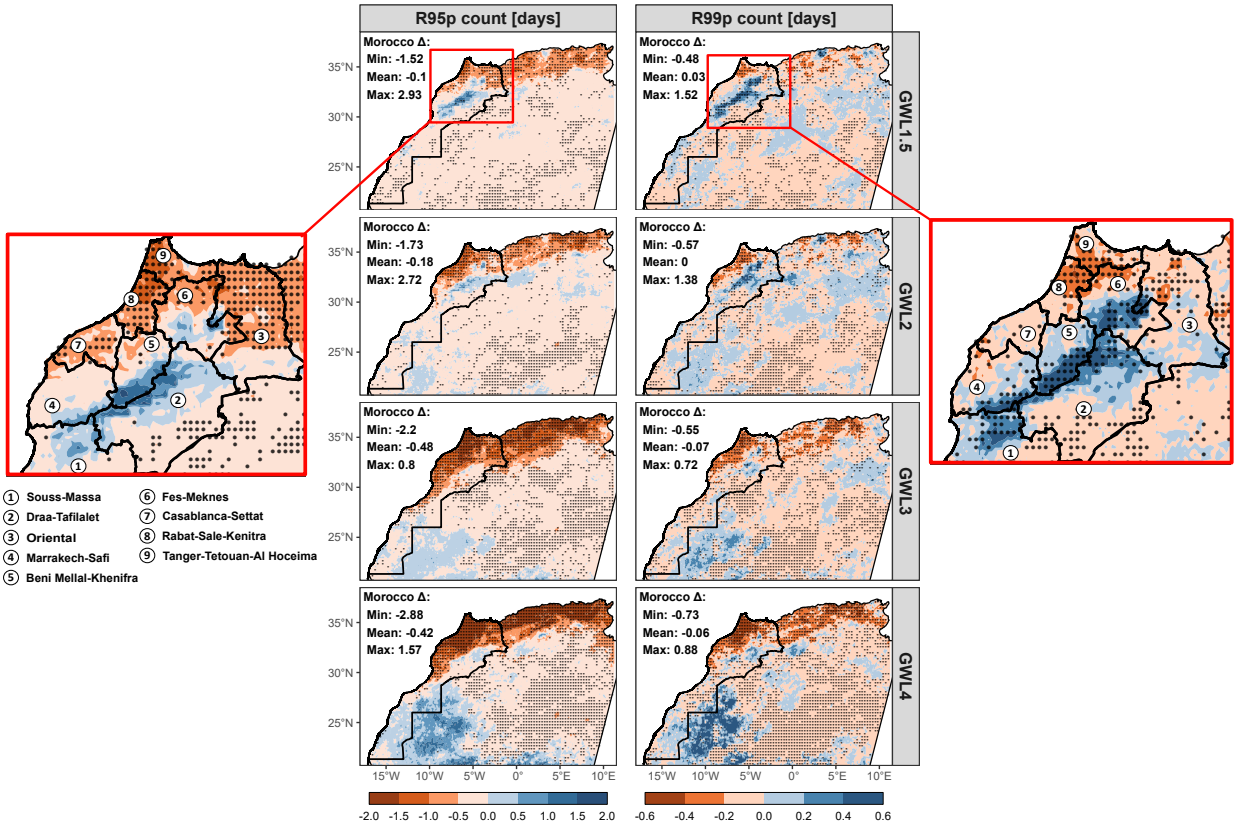


Figure 8: Ensemble-mean change in the annual count of days exceeding the 95th (`R95p`) and 99th (`R99p`) wet-day percentiles relative to the 1995–2014 reference period at fixed global warming levels (GWL1.5–GWL4°C). Only members available at each GWL are averaged; scenarios are first averaged within each model to avoid double-counting model effects. Stippling (black dots) marks pixels where all models agree on the sign of change. Annotated statistics are computed over Morocco only. Zoomed insets at GWL1.5°C show the regional detail within Morocco, with numbered labels corresponding to the administrative regions listed in the legend.

in very/extremely wet events. In contrast, September at GWL 4 shows a marked positive departure from the baseline; the large interquartile ranges and whiskers indicate substantial inter-model divergence in the magnitude and sign of change. This is consistent with occasional late-summer/early-autumn tropical-origin moisture intrusions affecting the southern/western sector of the domain, and with the maps of GWL 4 (Figure 9) that show localized increases over the southwest. The September GWL 4 maps of changes in EP events (Figure S12) confirms this pattern. At lower warming levels (GWL 1.5), Morocco shows a modest year-round enhancement of EP frequency. These early-warming increases correspond spatially to

the positive anomalies over the Atlas Mountains (Figure 9), indicating that orographically enhanced extremes may intensify temporarily before large-scale drying dominates at higher GWLs.

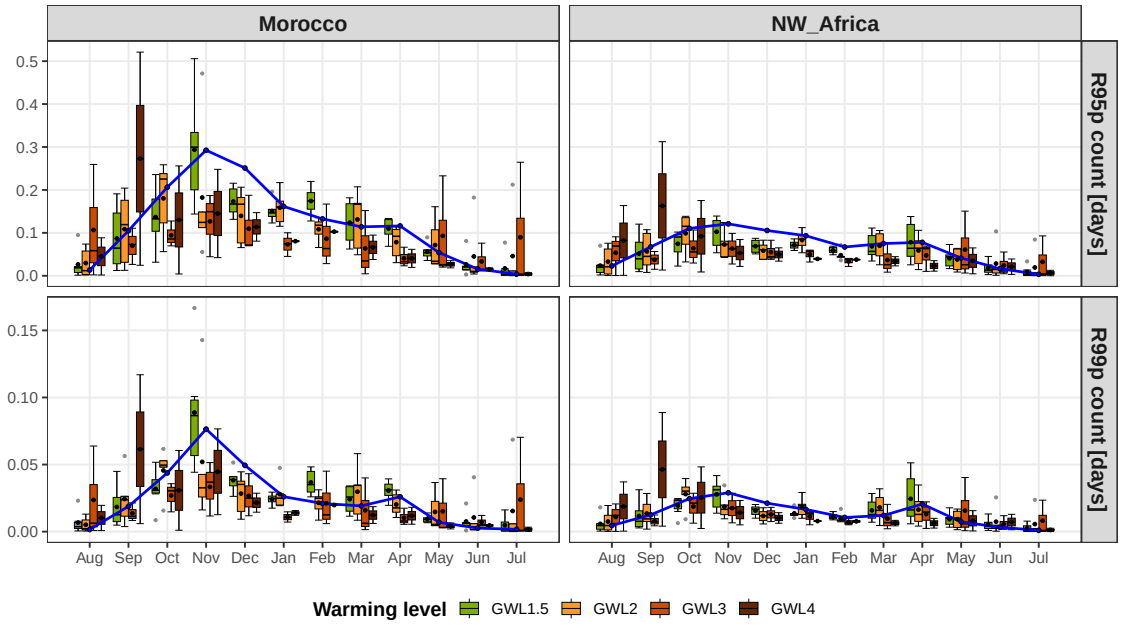


Figure 9: Ensemble spread of the mean seasonal cycle for each downscaled member of the frequency of EP events—`R95p` and `R99p`—across Northwest Africa and Morocco at fixed global warming levels (GWLs). The blue line denotes the 1995–2014 reference seasonal cycle (MSWEP); boxes show the interquartile range across members (model–scenario combinations), and black dots indicate the ensemble mean.

3.3.2 Change in intensity

Following the observed decline in the frequency of EP events, we now investigate changes in their intensity at fixed Global Warming Levels using three indices: wet-day mean intensity (`SDII`), annual 1-day maxima (`RX1day`), and annual wet-day totals (`PRCPTOT`). Morocco-averaged changes (Figure 10) first reveal a modest but consistent increase in `SDII` with warming, shown by ensemble means of +0.5 to +0.9 mm/day across GWL 1.5–4 and localized maxima up to +19.8 mm/day at GWL 4; this intensification is robust across all models and confined to the south of the Atlas Mountain ranges and the Sahara. However, in direct contrast, changes in `RX1day` mirror the declining frequency patterns of R99p and R95p (Figure 8), with the annual maximum 1-day precipitation decreasing from a Morocco-mean of −1 mm at

GWL 1.5 to −4 mm by GWL 4, and the largest decreases (∼ −10 to −25 mm/day) located along the Atlantic coast, the Anti-Atlas, and southeast of the High Atlas. Notably, against this domain-wide decline in `RX1day`, a localized increase is projected at the lowest warming level (GWL 1.5) across the interior regions (Draa-Tafilalet, Beni Mellal-Khenifra, Marrakech-Safi, and Fes-Meknes). As shown by the zoomed inset in Figure 10, the stippling over `RX1day` at GWL 1.5 is dense over these regions, indicating robust model agreement on this intensification. The trend of decreasing precipitation is further reinforced by the `PRCPTOT` index. Starting from a Morocco-mean climatology of ∼ 183 mm (Figure 7), the annual wet-day total shows a continuous decrease, with the ensemble-mean reduction escalating from −32 mm (−17%) at GWL 1.5 to −74 mm (−40%) at GWL 4, as models unanimously project this overall drying. In short, wet days get somewhat wetter on average, but annual maxima do not strengthen coherently, and annual totals decrease across the ensemble.

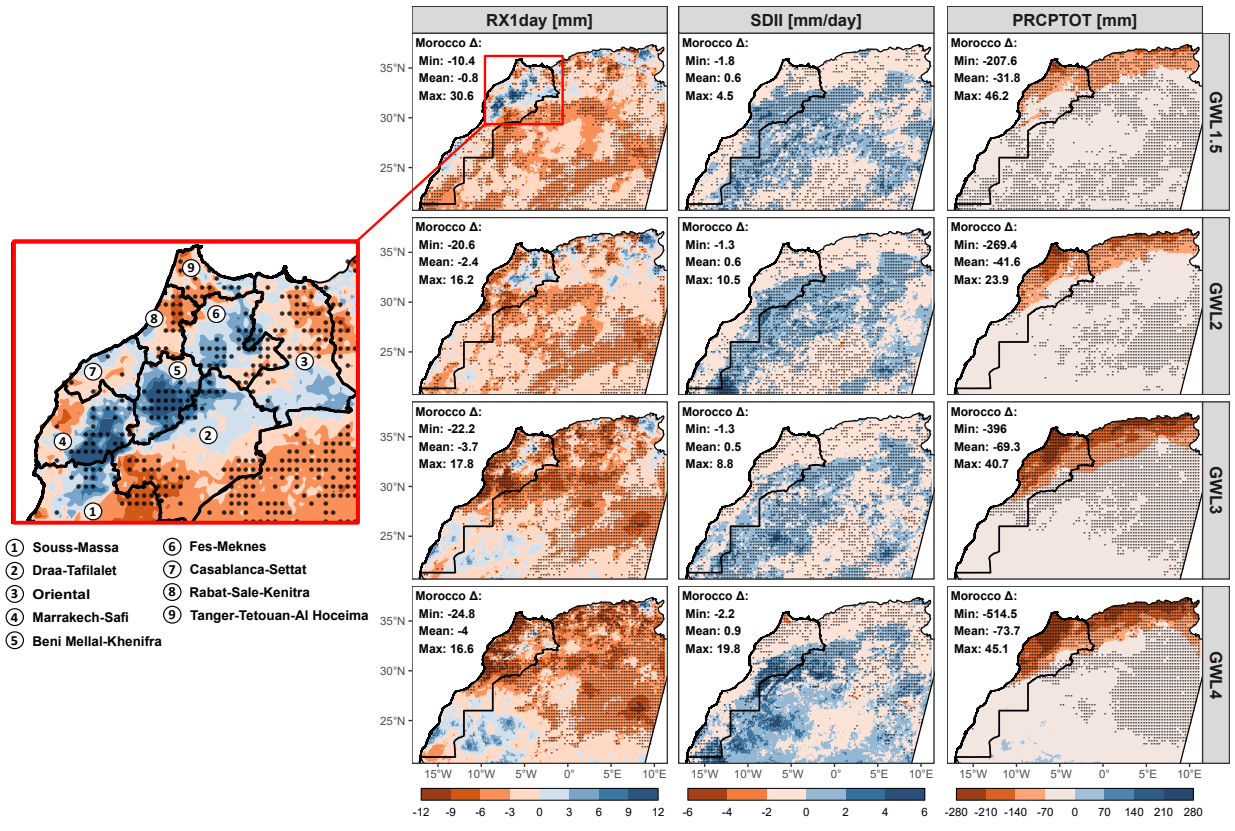


Figure 10: As in Figure 8, but for EP events intensity—`SDII`, `RX1day`, and `PRCPTOT`.

At the seasonal scale (Figure 11), the projected intensification of daily rainfall, measured by SDII, displays a distinct regional character. While both domains show a systematic increase above the reference climatology across most months and GWLs, the signal is significantly more robust and pronounced over the NW Africa domain. Here, nearly the entire interquartile range of the ensemble lies above the reference line, indicating a strong consensus on stronger extreme intensification, particularly over arid regions. In contrast, Morocco exhibits a more modest and seasonally variable intensification, with some models even projecting a slight decrease during specific months at higher GWLs. For PRCPTOT, the analysis reveals a coherent and concerning trend of drying. Despite the inherently low seasonal amplitude over the largely desert NW Africa domain, both regions exhibit a clear decline in total precipitation. The ensemble boxes and their whiskers predominantly shift below the reference line for all GWLs, with the most substantial drying concentrated in the core wet season months (November–February). The synthesis of these signals points to a fundamental shift in hydrological regime toward a more "all-or-nothing" character. This is characterized by wet days that are, on average, rainier (increasing SDII) but less frequent, resulting in lower annual precipitation totals (decreasing PRCPTOT). Critically, this intensification does not extend to extreme events, as we previously identified a general decline in annual maximum one-day precipitation (RX1day).

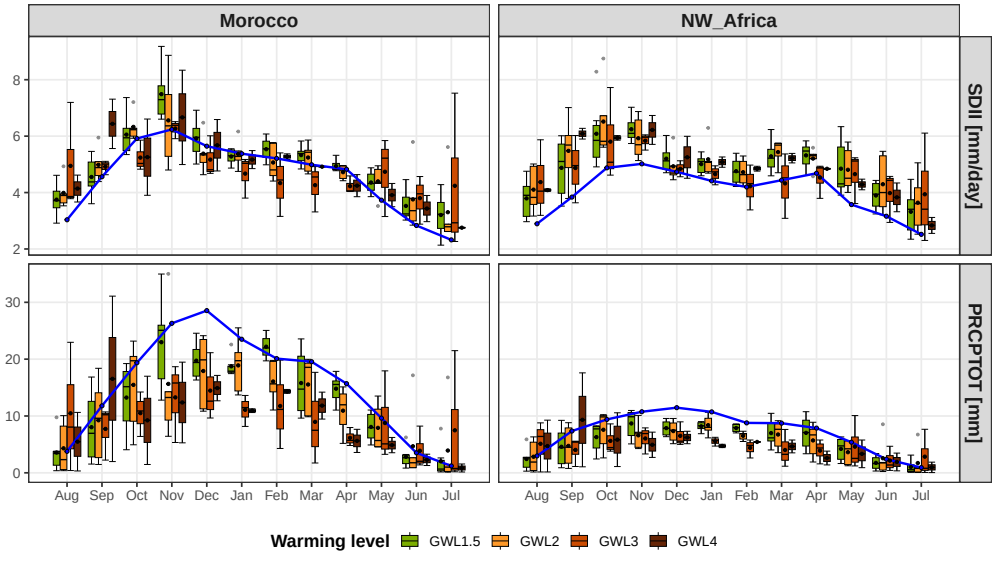


Figure 11: As in Figure 9, but for wet days intensity—SDII and PRCPTOT.

3.3.3 Change in contribution

The changes in EP contribution (`R95pTOT [mm]` and `R99pTOT [mm]`) exhibit a coherent, ridge-following pattern that closely mirrors the distribution of changes in EP events frequency (Figure 8). At lower warming levels (GWL 1.5–2), Atlas-centered increases dominate, particularly for `R99pTOT`. As highlighted by the zoomed insets in Figure 12, the `R99pTOT` increase at GWL 1.5 is accompanied by dense stippling across the interior and mountainous regions (Draa-Tafilalet, Beni Mellal-Khenifra, Marrakech-Safi, Souss-Massa and Fes-Meknes), confirming robust model agreement on this intensification. However, by GWL 3–4, this signal gives way to widespread drying concentrated along the coastal–orographic corridor from the Atlantic façade to the Kroumirie Mountains, where substantial reductions in heavy-tail precipitation amounts occur. These decreases show strong model agreement (stippling), indicating high confidence in the drying signal.

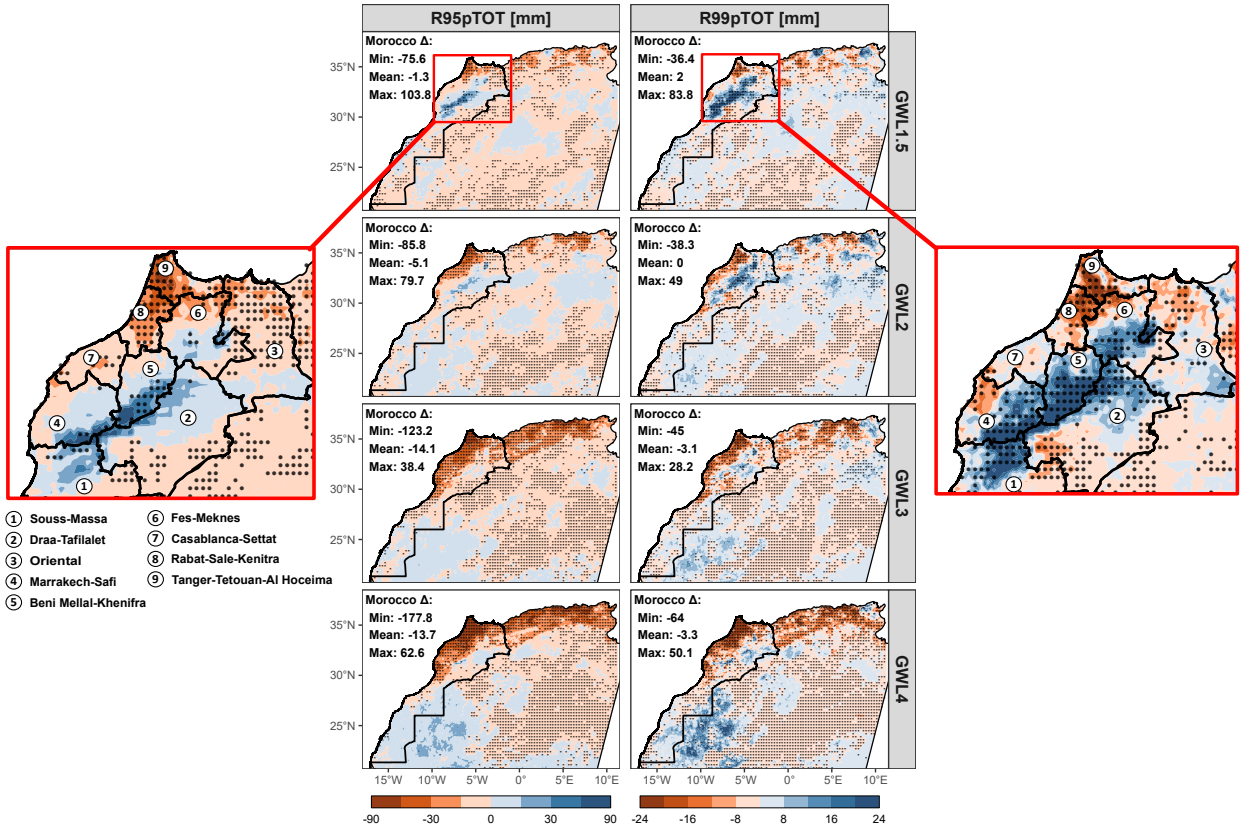


Figure 12: As in Figure 8, but for EP events contribution—`R95pTOT` and `R99pTOT`.

3.4 Extreme-Precipitation scaling with global warming

We summarize the sensitivity of extreme-precipitation indices to global warming as slopes fitted across GWL windows. Values in Table 5 report ensemble-mean slopes and model-range for Morocco and the full Northwest Africa domain. Table 5 reveals a coherent hydroclimatic shift across Morocco and Northwest Africa. Annual wet-day totals decline with warming (Morocco mean Δ`PRCPTOT` ≈ -17.8 mm/K). Wet-day mean intensity strengthens modestly (Δ`SDII` $\approx +0.09$ mm/day/K), yet the annual one-day maximum weakens on average (Δ`RX1day` ≈ -1.19 mm/K). Tail contributions decline consistently, with `R95pTOT` decreasing at ≈ -5.28 mm/K and `R99pTOT` at ≈ -2.14 mm/K, confirming that both the very-wet and extremely-wet fractions of precipitation shrink with warming, albeit more sharply for the broader very-wet-day category.

Table 5: Sensitivity (slope per K) of extreme precipitation indices to global warming levels (GWLs). Values are ensemble-mean slopes ("Mean") and per-model slope ranges ("Min.–Max.").

	Morocco			**NW Africa**		
Index (units/K)	**Min.**	**Max.**	**Mean**	**Min.**	**Max.**	**Mean**
RX1day (mm/K)	-2.15	0.25	-1.19	-0.82	0.94	-0.39
SDII (mm/day/K)	-0.07	0.13	0.09	-0.09	0.11	0.06
PRCPTOT (mm/K)	-17.61	-12.26	-17.80	-6.77	0.06	-5.53
R95pTOT (mm/K)	-6.41	-3.64	-5.28	-2.27	0.54	-1.38
R99pTOT (mm/K)	-2.56	-1.84	-2.14	-0.86	0.21	-0.55

4 Discussion

Our GWL-conditioned results over Northwest Africa and Morocco depict a coherent, two-stage hydroclimatic transition. The first stage, at lower warming levels (GWL1.5–2), is characterized by increasing EP, particularly over the Moroccan Atlas Mountains. We suggest that thermodynamic processes dominate during this initial phase, where atmospheric warming and moistening enhance orographic and convective processes, leading to more intense rainfall in accordance with established scaling relationships between EP and global warming (O'Gorman,

2015). This thermodynamic signal manifests as increasing trends in EP frequency (R95p, R99p), intensity (RX1day), and contribution (R95pTOT [mm], R99pTOT [mm]) over the Moroccan Atlas region, even as annual totals (PRCPTOT) show only decreasing trends across all GWLs.

The second stage emerges as dynamical forcing becomes dominant, driving a pronounced drying trend across the domain. This transition is explained by the mechanism of a strengthened and expanded Mediterranean anticyclonic anomaly in response to further warming, as demonstrated by Giorgi and Lionello (2008), Tuel and Eltahir (2020), and Tuel et al. (2021). This persistent anticyclone alters low-level circulation, promoting widespread subsidence over North Africa while advecting hot, dry Saharan air northwestward. The resulting pattern reduces lower-tropospheric humidity and suppresses Mediterranean cyclogenesis, ultimately producing robust cool-season (October–January) drying along the Atlantic–Mediterranean coastal–orographic corridor. At this stage, domain-wide decreasing trends emerge across all EP indices, including over the previously enhanced Moroccan Atlas region.

The two-stage EP response we identify, initial thermodynamic intensification followed by dynamically driven decline, is consistent with a body of observational and reanalysis-based evidence documenting a "hook" (or peak-like) relationship between extreme precipitation intensity and temperature across most land areas globally. In this relationship, EP increases with temperature up to a peak-point temperature (T_{pp}) and declines beyond it (Utsumi et al., 2011; Tian et al., 2023). Northwest Africa falls within the subtropical latitudinal band where this peak-like behaviour has been observed, and mountainous regions tend to have particularly low T_{pp} values (Utsumi et al., 2011), suggesting that the Atlas Mountains may reach their thermodynamic optimum for EP at relatively modest warming levels. The physical driver of the declining branch has been attributed to increasing atmospheric saturation deficit over land, which suppresses convective condensation as temperature rises faster than moisture supply can compensate (Sun and Wang, 2022). This interpretation is supported by the finding that when dew point temperature is used instead of surface air temperature, the negative

549 scaling largely vanishes, confirming moisture limitation as the controlling factor (Tian et al.,
550 2023). Although our analysis conditions EP in Northwest Africa on global mean surface
551 temperature rather than local temperature, as done in those studies, the structural similarity
552 between our projected two-stage transition and the globally documented "hook" structure
553 lends physical plausibility to our results and suggests that a similar thermodynamic constraint
554 may be operating. This is further corroborated by in-situ observations over Morocco, which
555 show that EP (RX1day) tends to increase, albeit with modest magnitudes, over the Moroccan
556 Atlas Mountains, while strongly declining in the extreme north of the country (Tuel and
557 Moçayd, 2023), a spatial pattern that closely mirrors the two-stage behavior projected here.

558 In addition to the strong inter-model agreement and the consistency of our findings
559 with previously reported signals in the literature, confidence in the projected EP signals is
560 supported by two key methodological strengths. First, the use of regional climate modeling at
561 10 km resolution enables improved representation of fine-scale processes—such as orographic
562 uplift, coastal gradients, and terrain-induced flow modifications—and has been shown to
563 substantially enhance the simulation of extremes over complex terrain compared to coarse-
564 resolution GCMs (Torma et al., 2015; Giorgi, 2019). Second, the application of a month-wise
565 quantile-mapping approach reduces seasonal and topographic biases, preserves the physically
566 driven change signal from the driving GCMs, and anchors the statistical distribution of
567 model simulations to the observed climate during the reference period, thereby enhancing
568 the realism of baseline conditions for assessing future changes. Collectively, these elements
569 indicate that the core results—namely, widespread drying in total precipitation alongside a
570 systematic intensification of extreme-day frequency, intensity, and contribution at low global
571 warming levels over the Moroccan Atlas Mountains—reflect robust model responses rather
572 than methodological artefacts.

5 Conclusions

This study evaluates projected changes in EP over Northwest Africa and Morocco under fixed global warming levels (GWLs of 1.5 °C to 4 °C). Across the full domain, the region is projected to undergo robust and progressive drying, quantified by a decline in annual precipitation of approximately −17.8 mm/K for Morocco, concurrent with a decreasing frequency of extreme events (e.g., Δ`R95p` ≈ -0.15 days/K) and a weakening of annual maximum one-day rainfall (Δ`RX1day` ≈ -1.19 mm/K), consistent with the Mediterranean large-scale circulation changes identified in Tuel et al. (2021) and Choi and Eltahir (2023).

Amid this widespread drying, the Moroccan Atlas Mountains exhibit a distinct two-stage hydroclimatic transition. At lower warming levels (GWL1.5–2), thermodynamic and orographic effects lead to a temporary intensification of precipitation extremes, with strong model agreement showing increased contributions from extreme events over interior and mountainous regions. However, as warming increases toward 3–4 °C, this signal reverses, with large-scale dynamical drying overriding the earlier thermodynamic intensification. This two-stage response is consistent with the "hook structure" widely documented in the global precipitation–temperature scaling literature, where EP peaks at an intermediate temperature before declining due to moisture limitation and increasing saturation deficit. The existence of this behaviour across diverse climatic regions and data sources lends physical plausibility to the nonlinear EP transition we project over the Moroccan Atlas.

Expressing EP changes per degree of warming allows risks to be assessed independently of the emission scenario or the timing at which warming levels are reached. In Morocco, the climate is shifting toward an "all-or-nothing" pattern, with fewer rainfall events but more intense storms. This raises the risk of flash floods over very dry soils, followed by longer periods of water scarcity. These results are important for regional water management and highlight the need to improve reservoir operations, drought preparedness, and flood protection. Future research should examine how stronger rainfall influences floods, soil moisture, and

599 groundwater recharge at 1.5 °C and 2 °C warming, particularly in vulnerable watersheds of
600 the Moroccan Atlas.

601 References

602 Abatzoglou, J. T., S. Z. Dobrowski, S. A. Parks, and K. C. Hegewisch, 2018: Terraclimate, a
603 high-resolution global dataset of monthly climate and climatic water balance from 1958–2015.
604 *Scientific Data*, **5**, 170 191, doi:10.1038/sdata.2017.191.

605 Babaousmail, H., R. Hou, B. Ayugi, M. Ojara, H. Ngoma, R. Karim, A. Rajasekar, and
606 V. Ongoma, 2021: Evaluation of the performance of cmip6 models in reproducing rainfall
607 patterns over north africa. *Atmosphere*, **12 (4)**, 475, doi:10.3390/atmos12040475.

608 Beck, H. E., E. F. Wood, M. Pan, C. K. Fisher, D. G. Miralles, A. I. Van Dijk, T. R. McVicar,
609 and R. F. Adler, 2019: Mswep v2 global 3-hourly 0.1 precipitation: methodology and
610 quantitative assessment. *Bulletin of the American Meteorological Society*, **100 (3)**, 473–500.

611 Bouaicha, R., and A. Benabdelfadel, 2010: Variabilité et gestion des eaux de surface au maroc.
612 *Sécheresse*, **21 (1e)**, 1–5.

613 Boucher, O., and Coauthors, 2020: Presentation and evaluation of the ipsl-cm6a-lr climate
614 model. *Journal of Advances in Modeling Earth Systems*, **12 (7)**, e2019MS002 010, doi:
615 10.1029/2019MS002010.

616 Cannon, A. J., S. R. Sobie, and T. Q. Murdock, 2015: Bias correction of gcm precipitation
617 by quantile mapping: How well do methods preserve changes in quantiles and extremes?
618 *Journal of Climate*, **28 (17)**, 6938–6959, doi:10.1175/JCLI-D-14-00754.1.

619 Chaqdid, A., A. Tuel, A. El Fatimy, and N. El Moçayd, 2023: Extreme rainfall events in

morocco: Spatial dependence and climate drivers. *Weather and Climate Extremes*, **40**, 100 556, URL https://doi.org/10.1016/j.wace.2023.100556.

Chaqdid, A., A. Tuel, A. El Fatimy, and N. El Moçayd, 2026: Towards reducing uncertainty in simulating temporal clustering of extreme precipitation in morocco: Insights from high-resolution gcms. *Journal of Climate*, e250138, URL https://doi.org/10.1175/JCLI-D-25-0138.1.

Choi, Y.-W., and E. A. Eltahir, 2023: Uncertainty in future projections of precipitation decline over mesopotamia. *Journal of Climate*, **36 (4)**, 1213–1228, URL https://doi.org/10.1175/JCLI-D-22-0268.1.

Cos, J., F. J. Doblas-Reyes, M. Jury, M. Marcos, P.-A. Bretonnière, and M. Samsó, 2022: The mediterranean climate change hotspot in the cmip5 and cmip6 projections. *Earth System Dynamics*, **13**, 321–340, doi:10.5194/esd-13-321-2022.

Döscher, R., and Coauthors, 2022: The ec-earth3 earth system model for the coupled model intercomparison project 6. *Geoscientific Model Development*, **15**, 2973–3020, doi:10.5194/gmd-15-2973-2022.

Dosio, A., and Coauthors, 2021: Projected future daily characteristics of african precipitation based on global (cmip5, cmip6) and regional (cordex, cordex-core) climate models. *Climate Dynamics*, **57 (11)**, 3135–3158.

Driouech, F., M. Déqué, and E. Sánchez-Gómez, 2010: Weather regimes—Moroccan precipitation link in a regional climate change simulation. *Global and Planetary Change*, **72 (1-2)**, 1–10, URL https://doi.org/10.1016/j.gloplacha.2010.03.004.

Dunn, R. J. H., L. V. Alexander, M. G. Donat, and Coauthors, 2020: Hadex3: A global land-

based dataset of climate extremes indices. *Journal of Geophysical Research: Atmospheres*, **125 (16)**, doi:10.1029/2019JD032263.

ETCCDI, 2009: Expert team on climate change detection and indices: Indices definitions. URL https://etccdi.pacificclimate.org/list_27_indices.shtml, accessed: 2025-10-08.

Filahi, S., M. Tanarhte, L. Mouhir, M. El Morhit, and Y. Tramblay, 2016: Trends in indices of daily temperature and precipitations extremes in morocco. *Theoretical and Applied Climatology*, **124 (3)**, 959–972, URL https://doi.org/10.1007/s00704-015-1472-4.

Foley, J. A., I. C. Prentice, N. Ramankutty, S. Levis, D. Pollard, S. Sitch, and A. Haxeltine, 1996: An integrated biosphere model of land surface processes, terrestrial carbon balance, and vegetation dynamics. *Global Biogeochemical Cycles*, **10 (4)**, 603–628, doi:10.1029/96GB02692.

Gadouali, F., N. Semane, Á. Muñoz, and M. Messouli, 2020: On the Link Between the Madden-Julian Oscillation, Euro-Mediterranean Weather Regimes, and Morocco Winter Rainfall. *Journal of Geophysical Research: Atmospheres*, **125 (8)**, e2020JD032 387, URL https://doi.org/10.1029/2020JD032387.

General Directorate of Meteorology, 2024: State of the climate in morocco 2024. Tech. rep., Kingdom of Morocco, Ministry of Equipment and Water. URL https://www.marocmeteo.ma/sites/default/files/climat_report/pdfs/Maroc_Etat_Climat_2024.pdf, accessed: 2025-11-05.

Gianotti, R. L., 2012: Convective organization and precipitation over the maritime continent: New insights from observation and modeling. Ph.D. thesis, Massachusetts Institute of Technology, URL https://dspace.mit.edu/handle/1721.1/71107.

Gianotti, R. L., and E. A. B. Eltahir, 2014a: Regional climate modeling over the maritime continent. part i: New parameterization for convective cloud fraction. *Journal of Climate*, **27 (4)**, 1488–1503, doi:10.1175/JCLI-D-13-00127.1.

Gianotti, R. L., and E. A. B. Eltahir, 2014b: Regional climate modeling over the maritime continent. part ii: New parameterization for autoconversion of convective rainfall. *Journal of Climate*, **27 (4)**, 1504–1523, doi:10.1175/JCLI-D-13-00171.1.

Giorgi, F., 2019: Thirty years of regional climate modeling: where are we and where are we going next? *Journal of Geophysical Research: Atmospheres*, **124 (11)**, 5696–5723.

Giorgi, F., and P. Lionello, 2008: Climate change projections for the Mediterranean region. *Global and planetary change*, **63 (2-3)**, 90–104, URL https://doi.org/10.1016/j.gloplacha.2007.09.005.

Gumus, V., N. El Moçayd, M. Seker, and M. Seaid, 2023: Assessment of cmip6 multi-model ensemble downscaled by artificial neural networks for morocco. *Atmospheric Research*, **289**, 106 783, doi:10.1016/j.atmosres.2023.106783.

Gutjahr, O., and G. Heinemann, 2013: Comparing precipitation bias correction methods for high-resolution regional climate simulations using cosmo-clm: Effects on extreme values and climate change signal. *Theoretical and Applied Climatology*, **114 (3)**, 511–529, doi:10.1007/s00704-013-0834-z.

Gutjahr, O., D. Putrasahan, K. Lohmann, J. H. Jungclaus, J.-S. von Storch, N. Brüggemann, H. Haak, and A. Stößel, 2019: Max planck institute earth system model (mpi-esm1.2) for the high-resolution model intercomparison project (highresmip). *Geoscientific Model Development*, **12 (7)**, 3241–3281, doi:10.5194/gmd-12-3241-2019.

686 Hawkins, E., and R. Sutton, 2009: The potential to narrow uncertainty in regional climate
687 predictions. *Bulletin of the American Meteorological Society*, **90 (8)**, 1095–1107, doi:
688 10.1175/2009BAMS2607.1.

689 Hersbach, H., and Coauthors, 2020: The ERA5 global reanalysis. *Quarterly Journal of the*
690 *Royal Meteorological Society*, **146 (730)**, 1999–2049, URL https://doi.org/10.1002/qj.3803.

691 Holtslag, A. A. M., and B. A. Boville, 1993: Local versus nonlocal boundary-layer diffusion in
692 a global climate model. *Journal of Climate*, **6 (10)**, 1825–1842, doi:10.1175/1520-0442(1993)
693 006⟨1825:LVNBLD⟩2.0.CO;2.

694 Hssaisoune, M., L. Bouchaou, A. Sifeddine, I. Bouimetarhan, and A. Chehbouni, 2020:
695 Morocco's groundwater resources and evolution with global climate changes. *Geosciences*,
696 **10 (2)**, 81, doi:10.3390/geosciences10020081.

697 Huffman, G. J., and Coauthors, 2007: The trmm multisatellite precipitation analysis (tmpa):
698 Quasi-global, multiyear, combined-sensor precipitation estimates at fine scales. *Journal of*
699 *Hydrometeorology*, **8 (1)**, 38–55, doi:10.1175/JHM560.1.

700 Im, E.-S., R. L. Gianotti, and E. A. B. Eltahir, 2014: Improving the simulation of the
701 west african monsoon using the mit regional climate model. *Journal of Climate*, **27 (6)**,
702 2209–2229, doi:10.1175/JCLI-D-13-00188.1.

703 IPCC, 2022: Climate Change 2022: Impacts, Adaptation, and Vulnerability. Contribution
704 of Working Group II to the Sixth Assessment Report of the Intergovernmental Panel on
705 Climate Change [H.-O. Pörtner, D.C. Roberts, M. Tignor, E.S. Poloczanska, K. Mintenbeck,
706 A. Alegría, M. Craig, S. Langsdorf, S. Löschke, V. Möller, A. Okem, B. Rama (eds.)].
707 *Cambridge University Press*.

Khomsi, K., G. Mahe, Y. Tramblay, M. Sinan, and M. Snoussi, 2016: Regional impacts of global change: seasonal trends in extreme rainfall, run-off and temperature in two contrasting regions of Morocco. *Natural Hazards and Earth System Sciences*, **16 (5)**, 1079–1090, URL https://doi.org/10.5194/nhess-16-1079-2016.

Kiehl, J. T., J. J. Hack, G. B. Bonan, B. A. Boville, D. L. Williamson, and P. J. Rasch, 1998: The national center for atmospheric research community climate model: Ccm3. *Journal of Climate*, **11 (6)**, 1131–1149, doi:10.1175/1520-0442(1998)011⟨1131:TNCFAR⟩2.0.CO;2.

Kissami, I., R. Basmadjian, O. Chakir, and M. R. Abid, 2025: Toubkal: a high-performance supercomputer powering scientific research in africa. *The Journal of Supercomputing*, **81 (15)**, 1–45, URL https://doi.org/10.1007/s11227-025-07858-8.

Lenderink, G., A. Buishand, and W. Van Deursen, 2007: Estimates of future discharges of the river rhine using two scenario methodologies: direct versus delta approach. *Hydrology and Earth System Sciences*, **11 (3)**, 1145–1159, doi:10.5194/hess-11-1145-2007.

Maraun, D., 2013: Bias correction, quantile mapping, and downscaling: Revisiting the inflation issue. *Journal of Climate*, **26 (6)**, 2137–2143.

Maraun, D., 2016: Bias correcting climate change simulations—a critical review. *Current Climate Change Reports*, **2**, 211–220, doi:10.1007/s40641-016-0050-x.

Marcella, M. P., and E. A. B. Eltahir, 2012: Modeling the summertime climate of southwest asia: The role of land surface processes in shaping the climate of semiarid regions. *Journal of Climate*, **25 (2)**, 704–719, doi:10.1175/2011JCLI4080.1.

Marcella, M. P., and E. A. B. Eltahir, 2014: Introducing an irrigation scheme to a regional climate model: A case study over west africa. *Journal of Climate*, **27 (15)**, 5708–5723,

doi:10.1175/JCLI-D-13-00116.1.

O'Gorman, P. A., 2009: Scaling of precipitation extremes over a wide range of climates simulated with an idealized gcm. *Journal of Climate*, **22 (21)**, 5676–5685, doi:10.1175/2009JCLI2701.1.

O'Gorman, P. A., 2015: Precipitation extremes under climate change. *Current Climate Change Reports*, **1**, 49–59, doi:10.1007/s40641-015-0009-3.

Pal, J. S., and E. A. B. Eltahir, 2016: Future temperature in southwest asia projected to exceed a threshold for human adaptability. *Nature Climate Change*, **6**, 197–200, doi:10.1038/nclimate2833.

Pal, J. S., F. Giorgi, X. Bi, N. Elguindi, F. Solmon, X. Gao, and Coauthors, 2007: Regional climate modeling for the developing world: The ictp regcm3 and regcnet. *Bulletin of the American Meteorological Society*, **88 (9)**, 1395–1409, doi:10.1175/BAMS-88-9-1395.

Pal, J. S., E. E. Small, and E. A. B. Eltahir, 2000: Simulation of regional-scale water and energy budgets: Representation of subgrid cloud and precipitation processes within regcm. *Journal of Geophysical Research: Atmospheres*, **105 (D24)**, 29 579–29 594, doi:10.1029/2000JD900415.

Piani, C., J. O. Haerter, and E. Coppola, 2010: Statistical bias correction for daily precipitation in regional climate models over europe. *Theoretical and Applied Climatology*, **99 (1)**, 187–192, doi:10.1007/s00704-009-0134-9.

Reiter, P., O. Gutjahr, L. Schefczyk, G. Heinemann, and M. Casper, 2016: Bias correction of ensembles precipitation data with focus on the effect of the length of the calibration period. *Meteorologische Zeitschrift*, **25**, 85–96.

Reynolds, R. W., N. A. Rayner, T. M. Smith, D. C. Stokes, and W. Wang, 2002: An improved in situ and satellite sst analysis for climate. *Journal of Climate*, **15 (13)**, 1609–1625, doi:10.1175/1520-0442(2002)015⟨1609:AIISAS⟩2.0.CO;2.

Schmidli, J., C. Frei, and P. L. Vidale, 2006: Downscaling from gcm precipitation: a benchmark for dynamical and statistical downscaling methods. *International Journal of Climatology*, **26 (5)**, 679–689, doi:10.1002/joc.1287.

Seneviratne, S. I., and Coauthors, 2021: Weather and climate extreme events in a changing climate. *Climate Change 2021: The Physical Science Basis. Contribution of Working Group I to the Sixth Assessment Report of the IPCC*, V. Masson-Delmotte, P. Zhai, A. Pirani, S. L. Connors, C. Péan, S. Berger, N. Caud, Y. Chen, L. Goldfarb, M. I. Gomis et al., Eds., Cambridge University Press, Cambridge, UK and New York, USA, URL https://www.cambridge.org/core/books/climate-change-2021-the-physical-science-basis/weather-and-climate-extreme-events-in-a-changing-climate/2F83F3B7E10AFB12F949BA80C1B02C1B.

Sun, X., and G. Wang, 2022: Causes for the negative scaling of extreme precipitation at high temperatures. *Journal of Climate*, **35 (18)**, 6119–6134, doi:10.1175/JCLI-D-22-0142.1.

Taylor, R. G., M. C. Todd, L. Kongola, L. Maurice, E. Nahozya, H. Sanga, and A. M. MacDonald, 2013: Evidence of the dependence of groundwater resources on extreme rainfall in east africa. *Nature Climate Change*, **3 (4)**, 374–378, doi:10.1038/nclimate1731.

Themeßl, M. J., A. Gobiet, and G. Heinrich, 2012: Empirical-statistical downscaling and error correction of regional climate models and its impact on the climate change signal. *Climatic Change*, **112 (2)**, 449–468, doi:10.1007/s10584-011-0224-4.

Tian, B., H. Chen, J. Yin, Z. Liao, N. Li, and S. He, 2023: Global scaling of precipitation

extremes using near-surface air temperature and dew point temperature. *Environmental Research Letters*, **18 (3)**, 034 016, doi:10.1088/1748-9326/acb836.

Torma, C., F. Giorgi, and E. Coppola, 2015: Added value of regional climate modeling over areas characterized by complex terrain—precipitation over the alps. *Journal of Geophysical Research: Atmospheres*, **120 (9)**, 3957–3972, doi:10.1002/2014JD022781.

Tramblay, Y., W. Badi, F. Driouech, S. El Adlouni, L. Neppel, and E. Servat, 2012: Climate change impacts on extreme precipitation in Morocco . *Global and Planetary change*, **82**, 104–114, URL https://doi.org/10.1016/j.gloplacha.2011.12.002.

Tramblay, Y., D. Ruelland, S. Somot, R. Bouaicha, and E. Servat, 2013: High-resolution med-cordex regional climate model simulations: evaluation and hydrological applications in morocco. *Hydrology and Earth System Sciences*, **17 (9)**, 3721–3739, doi:10.5194/hess-17-3721-2013.

Tramblay, Y., and S. Somot, 2018: Future evolution of extreme precipitation in the mediterranean. *Climatic Change*, **151**, 289–302, doi:10.1007/s10584-018-2300-5.

Tuel, A., N. El Moçayd, M. D. Hasnaoui, and E. A. B. Eltahir, 2022: Future projections of high atlas snowpack and runoff under climate change. *Hydrology and Earth System Sciences*, **26 (3)**, 571–588, doi:10.5194/hess-26-571-2022.

Tuel, A., and E. A. B. Eltahir, 2020: Why is the mediterranean a climate change hot spot? *Journal of Climate*, **33 (14)**, 5829–5843, doi:10.1175/JCLI-D-19-0910.1.

Tuel, A., S. Kang, and E. A. B. Eltahir, 2021: Understanding climate change over the southwestern mediterranean using high-resolution simulations. *Climate Dynamics*, **56 (3)**, 985–1001.

Tuel, A., and N. E. Moçayd, 2023: Evaluating extreme precipitation in gridded datasets with a novel station database in morocco. doi:10.22541/essoar.167525285.54960295/v1, URL https://doi.org/10.22541%2Fessoar.167525285.54960295%2Fv1.

UNFCCC, 2015: Adoption of the paris agreement, fccc/cp/2015/l.9/rev.1. *United Nations Framework Convention on Climate Change*, URL https://unfccc.int/resource/docs/2015/cop21/eng/l09r01.pdf.

Utsumi, N., S. Seto, S. Kanae, E. E. Maeda, and T. Oki, 2011: Does higher surface temperature intensify extreme precipitation? *Geophysical Research Letters*, **38 (16)**, L16 708, doi: 10.1029/2011GL048426.

Winter, J. M., J. S. Pal, and E. A. B. Eltahir, 2009: Coupling of integrated biosphere simulator to regional climate model version 3. *Journal of Climate*, **22 (10)**, 2743–2757, doi:10.1175/2008JCLI2541.1.

Zeng, X., M. Zhao, and R. E. Dickinson, 1998: Intercomparison of bulk aerodynamic algorithms for the computation of sea surface fluxes using toga coare and tao data. *Journal of Climate*, **11 (10)**, 2628–2644, doi:10.1175/1520-0442(1998)011⟨2628:IOBAAF⟩2.0.CO;2.

Statements and Declarations

Funding

This work was conducted within the framework of the UMRP project. The authors gratefully acknowledge the financial support provided by OCP. The computations were performed using the High Performance Computing facilities of the Toubkal supercomputer (Kissami et al., 2025) at Mohammed VI Polytechnic University, Benguerir.

Competing Interests

The authors have no conflicts of interest to disclose.

Author Contributions

All authors contributed to the study conception and design. Material preparation, data collection, and analysis were performed A. C and Y. C. The first draft of the manuscript was written by A. C, and all authors commented on previous versions of the manuscript. All authors read and approved the final manuscript.

Data Availability

The main datasets used in this study are publicly available and can be accessed as follows:

- **ERA5 reanalysis data**: ERA5 data are available from the Copernicus Climate Data Store at: https://cds.climate.copernicus.eu/.

- **CMIP6 simulations**: Data from the CMIP6 project are accessible via the Earth System Grid Federation (ESGF) data portal at: https://wcrp-cmip.org/cmip-data-access/, under the CMIP6 collection.

- **MSWEP precipitation data**: The Multi-Source Weighted-Ensemble Precipitation

(MSWEP) dataset is available at: https://www.gloh2o.org/mswep/.

The datasets generated during the current study are available from the corresponding author on reasonable request.